Human Molecular Genetics, 2018, Vol. 27, No. 8 1396–1410

doi: 10.1093/hmg/ddy050
Advance Access Publication Date: 8 February 2018
Original Article

ORIGINAL ARTICLE

Protein kinase C activity is a protective modifier of Purkinje neuron degeneration in cerebellar ataxia

Ravi Chopra[1,2,3], Aaron H. Wasserman[3], Stefan M. Pulst[4], Chris I. De Zeeuw[5,6] and Vikram G. Shakkottai[3,7,*]

[1]Medical Scientist Training Program, University of Michigan Medical School, Ann Arbor, MI 48109, USA, [2]Neuroscience Graduate Program, University of Michigan, Ann Arbor, MI 48109, USA, [3]Department of Neurology, University of Michigan Medical School, Ann Arbor, MI 48109, USA, [4]Department of Neurology, University of Utah, Salt Lake City, UT 84132, USA, [5]Netherlands Institute for Neuroscience, Amsterdam 1105 CA, The Netherlands, [6]Department of Neuroscience, Erasmus MC, Rotterdam 3015 GE, The Netherlands and [7]Department of Molecular and Integrative Physiology, University of Michigan, Ann Arbor, MI 48109, USA

*To whom correspondence should be addressed at: 4009 BSRB, 109 Zina Pitcher Place, Ann Arbor, MI 48109, USA. Tel: 734-615-6891; Fax: 734-647-9777; Email: vikramsh@med.umich.edu

Abstract

Among the many types of neurons expressing protein kinase C (PKC) enzymes, cerebellar Purkinje neurons are particularly reliant on appropriate PKC activity for maintaining homeostasis. The importance of PKC enzymes in Purkinje neuron health is apparent as mutations in *PRKCG* (encoding PKCγ) cause cerebellar ataxia. *PRKCG* has also been identified as an important node in ataxia gene networks more broadly, but the functional role of PKC in other forms of ataxia remains unexplored, and the mechanisms by which PKC isozymes regulate Purkinje neuron health are not well understood. Here, we investigated how PKC activity influences neurodegeneration in inherited ataxia. Using mouse models of spinocerebellar ataxia type 1 (SCA1) and 2 (SCA2) we identify an increase in PKC-mediated substrate phosphorylation in two different forms of inherited cerebellar ataxia. Normalizing PKC substrate phosphorylation in SCA1 and SCA2 mice accelerates degeneration, suggesting that the increased activity observed in these models is neuroprotective. We also find that increased phosphorylation of PKC targets limits Purkinje neuron membrane excitability, suggesting that PKC activity may support Purkinje neuron health by moderating excitability. These data suggest a functional role for PKC enzymes in ataxia gene networks, and demonstrate that increased PKC activity is a protective modifier of degeneration in inherited cerebellar ataxia.

Introduction

Cerebellar ataxias are a heterogeneous group of disorders with degeneration in the cerebellum and its connections (1,2). Diverse genetic forms of ataxia produce a shared pattern of degeneration of cerebellar neurons, and in many cases a profound loss of cerebellar Purkinje neurons. The basis for the vulnerability of cerebellar Purkinje neurons in ataxia is unclear. Recent work has identified altered membrane excitability as one of the mechanisms for Purkinje neuron vulnerability in ataxia (3). This is supported by genetic causes of ataxia that result from mutations in ion channels that regulate membrane excitability, as well as identification of alterations in ion channel expression and function in other causes of ataxia not directly related to ion channel mutations (4). Cerebellar ataxia can also result from alterations in signaling

Received: November 16, 2017. **Revised:** January 30, 2018. **Accepted:** February 5, 2018

pathways important for Purkinje neuron function. The relationship between membrane excitability and these signaling pathways remains unexplored.

Protein kinase C (PKC) enzymes are a family of serine/threonine kinases with widespread expression throughout the brain (5). They play important roles in synaptic function, ion channel regulation, neurite outgrowth, synaptic plasticity and in learning and memory (6). The expression of several PKC isozymes is particularly enriched in the cerebellum, where PKC activity plays an important role in normal Purkinje neuron function (7). *In vitro* studies have shown that phorbol esters that activate PKC enzymes produce profound impairment in Purkinje neuron dendrite development (8). Furthermore, mutations in *PRKCG*, encoding the PKCγ isozyme, cause spinocerebellar ataxia type 14 (SCA14) (9–11), a form of cerebellar ataxia with selective Purkinje neuron degeneration (12) despite widespread expression of PKCγ (5). Increased enzyme function (13), novel gain of function (14,15) and reduced enzyme function (16) have all been proposed as mechanisms by which *PRKCG* mutations produce Purkinje neuron pathology. Finally, analysis of gene coexpression in human cerebellar tissue has revealed that *PRKCG* is a node in an interrelated module for many ataxia-linked genes (17), and protein products of the ataxia-linked genes *ITPR1* (codes for the type 1 IP3 receptor, implicated in SCA15/16), *TRPC3* (codes for TRPC3, implicated in SCA41) and *KCNC3* (codes for Kv3.3, implicated in SCA13) are already known to be PKC substrates (16,18,19). Taken together, these findings suggest that appropriate PKC activity is critical for maintaining Purkinje neuron homeostasis, and they raise the possibility that altered PKC activity could play a role in forms of cerebellar ataxia beyond SCA14.

Given the importance of PKC enzymes in Purkinje neuron health and the data suggesting that PKC enzymes are a node in ataxia gene networks, we hypothesized that PKC activity might influence degeneration in inherited and sporadic ataxias more broadly. Using mouse models of spinocerebellar ataxia type 1 (SCA1) and spinocerebellar ataxia type 2 (SCA2) as well as patient autopsy tissue from SCA1 and multiple system atrophy (MSA), we demonstrate that increased PKC activity can be observed in several forms of cerebellar ataxia. We demonstrate that this activity is mediated by conventional PKC isozymes, implicating PKCα and/or PKCγ, and that it occurs in association with changes in DAG metabolism. Inhibiting PKC activity results in accelerated Purkinje neuron degeneration in SCA1 and SCA2 mouse models, suggesting that increasing PKC activity is neuroprotective in these forms of cerebellar ataxia. Finally, we demonstrate that increased PKC activity reduces Purkinje neuron membrane excitability, suggesting that PKC activity may influence neurodegeneration through its ability to modulate ion channel function. These findings establish a novel role for PKC activity as a modifier of neurodegeneration in forms of cerebellar ataxia not caused by PKC gene mutations.

Results

Increased PKC substrate phosphorylation is observed in SCA1

We wished to examine alterations in Purkinje neuron PKC activity associated with neurodegeneration in SCA1. Previous studies in the ATXN1[82Q] model of SCA1, a transgenic model where glutamine-expanded ATXN1 is expressed solely in Purkinje neurons, have demonstrated that motor impairment begins at 5 weeks of age in the absence of significant degeneration (20,21). We therefore first examined PKC activity in 5-week-old ATXN1[82Q]$^{tg/tg}$ mice. Since not all substrates of PKC have been identified, in order to investigate alterations in PKC activity, we used an antibody that recognizes phosphorylated serine residues within the PKC consensus motif on substrates (22). PKC substrate phosphorylation was increased in ATXN1[82Q]$^{tg/tg}$ cerebella (Fig. 1A and B) (wild type: 1.00 ± 0.03 AU, ATXN1[82Q]$^{tg/tg}$: 2.17 ± 0.16 AU). Progressive dendritic degeneration is evident in ATXN1[82Q]$^{tg/tg}$ Purkinje neurons at 15 weeks of age without cell loss (21,23). PKC activity was also increased at 15 weeks of age (Fig. 1C and D) (wild type: 1.00 ± 0.18 AU, ATXN1[82Q]$^{tg/tg}$: 2.49 ± 0.39 AU), demonstrating that increased PKC substrate phosphorylation is observed throughout the course of Purkinje neuron degeneration. Immunohistochemistry with the same antibody revealed very strong signal in Purkinje neurons relative to other cerebellar cell types (Fig. 1E), suggesting that a significant portion of the observed immunoblot signal originates from Purkinje neurons. Use of PKC inhibitors in organotypic cerebellar slice cultures reduces the immunoblot signal (Supplementary Material, Fig. S1A), supporting the conclusion that signal detected using this antibody is an indicator of steady-state phosphorylation of substrates by PKC enzymes.

Since the specificity of this antibody for labeling only substrates phosphorylated by PKC isozymes is unknown, we also confirmed this increase in PKC activity by assessing the phosphorylation of Ser^{880} on the GluA2 AMPA receptor subunit, a known PKC substrate (24) that is highly enriched in cerebellar Purkinje neurons (25). Phosphorylation of Ser^{880} on GluA2 was significantly elevated in ATXN1[82Q]$^{tg/tg}$ Purkinje neurons at 15 weeks (Fig. 1F and G) (wild type: 1.00 ± 0.09 AU, ATXN1[82Q]$^{tg/tg}$: 1.62 ± 0.22 AU). These data lend further support to the conclusion that Purkinje neuron PKC activity is increased in ATXN1[82Q]$^{tg/tg}$ mice.

The relevance of the observed increases in PKC activity to human disease was confirmed using post-mortem tissue from patients with SCA1 (Fig. 1H) (demographics summarized in Supplementary Material, Table S1). Consistent with the findings in ATXN1[82Q]$^{tg/tg}$ mice, there was a statistically significant increase in the ratio of phosphorylated PKC substrates relative to calbindin in the somata of SCA1 Purkinje neurons compared to healthy controls (Fig. 1I) (control: 0.85 AU, SCA1: 2.12 AU). The increase in PKC substrate staining was not restricted to Purkinje neurons in SCA1 patient samples, consistent with widespread expression of mutant ATXN1 (26). This increase could not be explained by a change in calbindin levels, as calbindin staining intensity was statistically indistinguishable between the two groups (Supplementary Material, Fig. S1B) (control: 1216.74 AU, SCA1: 1220.59 AU). Importantly, the staining intensity for phosphorylated PKC substrates was by itself significantly increased in SCA1 Purkinje neurons (Fig. 1J) (control: 979.40 AU, SCA1: 1584.08 AU). These findings support the conclusion that there is increased PKC substrate phosphorylation in Purkinje neurons from SCA1 patient autopsy tissue. There was a notable variability within the SCA1 patient samples, with several samples showing elevated phosphorylated PKC substrate-to-calbindin ratios. PKC substrate-to-calbindin ratio did not correlate with age of death or CAG repeat length (data not shown). Thus, while the significance of this variability remains unclear, the increase in PKC substrate phosphorylation in human autopsy tissue from SCA1 nevertheless supports the conclusion that PKC activity could play a role in modifying Purkinje neuron degeneration in patients with SCA1.

The PKC family of enzymes is subdivided into four subfamilies that are distinguished by the regulatory signals to which they respond (27). The conventional PKC isozyme subfamily (made up of PKCα, PKCβI/II and PKCγ) requires Ca^{2+} for activation. Cerebellar organotypic slice culture experiments

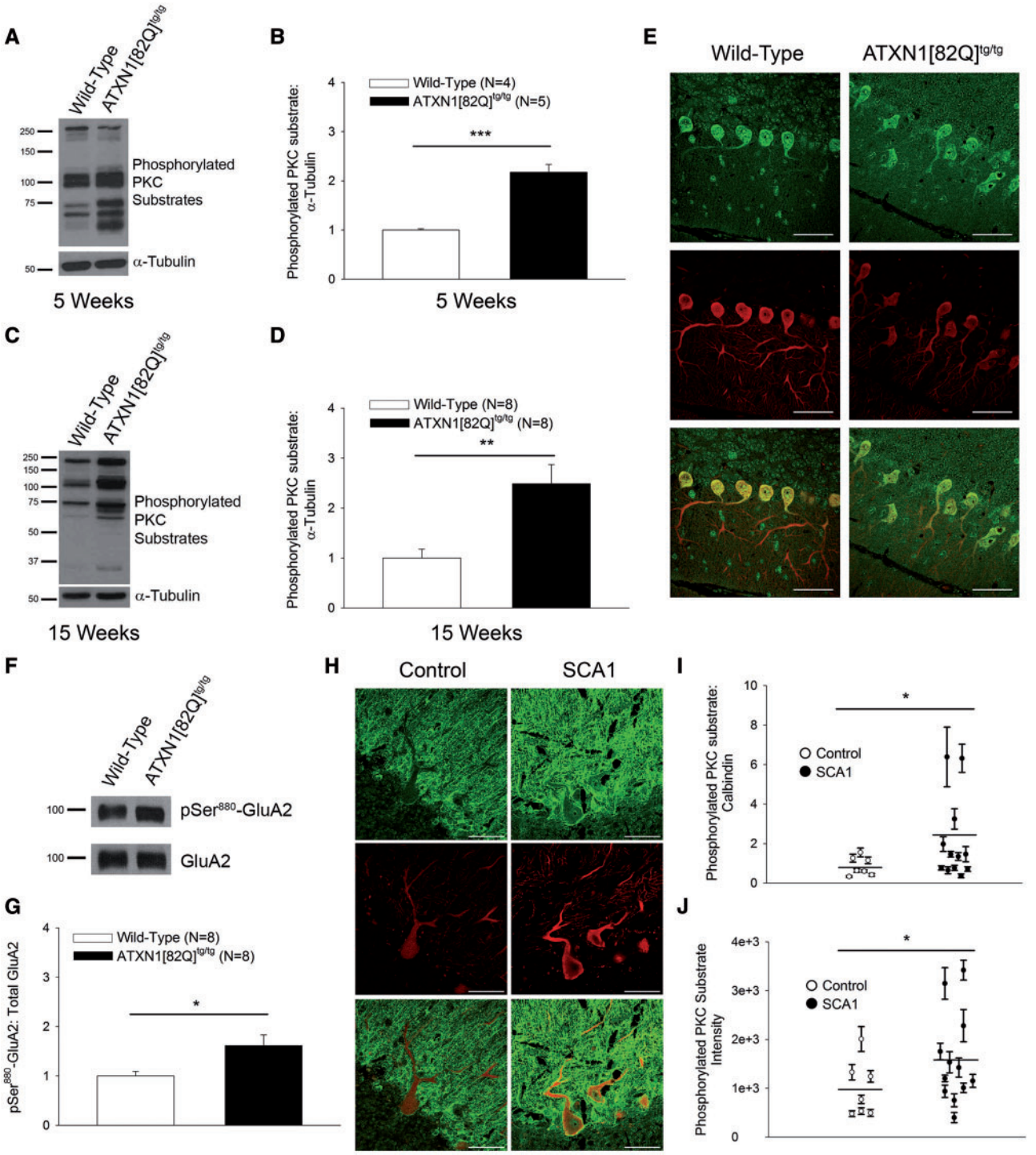

Figure 1. Increased cerebellar PKC substrate phosphorylation is observed in SCA1. (**A**) Representative western blot for phosphorylated PKC substrates at 5 weeks of age showing increased PKC substrate phosphorylation in cerebella from ATXN1[82Q]$^{tg/tg}$ mice, summarized in (**B**). Tubulin was used as a loading control. (**C**) Representative western blot for phosphorylated PKC substrates at 15 weeks of age show increased PKC substrate phosphorylation in cerebella from ATXN1[82Q]$^{tg/tg}$ mice, summarized in (**D**). Tubulin was used as a loading control. (**E**) Representative immunohistochemistry experiment showing PKC substrate phosphorylation (green) in Purkinje neurons (Calbindin: red) from the anterior cerebellar vermis in 15-week-old wild-type and ATXN1[82Q]$^{tg/tg}$ mice. Scale bars, 50 μm. (**F**) Western blot demonstrating increased phosphorylation of Ser^{880} of GluA2 in ATXN1[82Q]$^{tg/tg}$ mice at 15 weeks of age, summarized in (**G**). Total GluA2 was used as a loading control. (**H**) Representative images of phosphorylated PKC substrate staining (green) in calbindin-stained (red) Purkinje neurons from an SCA1 patient sample and healthy control sample. Scale bars, 50 μm. (**I**) Summarized data show an increase in phosphorylated PKC substrate-to-calbindin staining ratio in the somatic compartment of Purkinje neurons from SCA1 patient samples and age-matched healthy control samples. Each data point represents an individual patient, with error bars representing SEM for measurements from multiple Purkinje neurons in that individual. (**J**) Phosphorylated PKC substrate staining intensity in the somatic compartment shows a significant increase in SCA1 patient samples relative to age-matched healthy control samples. Each data point represents an individual patient, with error bars representing S.E.M. for measurements from multiple Purkinje neurons in that individual. Throughout, data are represented as means with error bars representing S.E.M. * $P<0.05$, ** $P<0.01$; *** $P<0.001$. Statistical significance derived by unpaired two-tailed Student's *t*-test (B, D, G) or two-way ANOVA (I, J).

from ATXN1[82Q]$^{tg/tg}$ and WT mice revealed that the increased PKC activity which was observed in SCA1 Purkinje neurons at 15 weeks could be eliminated by using 5 mM ethylene glycol-bis(β-aminoethyl ether)-N,N,N′,N′-tetraacetic acid (EGTA) to chelate extracellular Ca^{2+} ions (Fig. 2A and B) (wild-type control: 1.00 ± 0.15 AU, wild-type EGTA: 0.59 ± 0.08 AU, ATXN1[82Q]$^{tg/tg}$ control: 1.25 ± 0.20 AU, ATXN1[82Q]$^{tg/tg}$ EGTA: 0.60 ± 0.08 AU). This suggests that the observed change in PKC substrate phosphorylation is mediated by one of the conventional PKC isozymes. Purkinje neurons express both PKCα and PKCγ (28,29). ATXN1[82Q]$^{tg/tg}$ Purkinje neurons show unchanged PKCα expression (wild type: 1.00 ± 0.09 AU, ATXN1[82Q]$^{tg/tg}$: 1.15 ± 0.07 AU) and reduced PKCγ expression (wild type: 1.00 ± 0.03 AU, ATXN1[82Q]$^{tg/tg}$: 0.39 ± 0.03 AU), consistent with previous reports (30) (Fig. 2C–E and Supplementary Material, Fig. S2A and B). These data indicate that the observed increases in conventional PKC substrate phosphorylation cannot be explained by changes in expression of conventional PKC isozymes, and are likely due to increased activation of conventional PKC isozymes.

Calcium imaging studies in Purkinje neurons from the ATXN1[82Q] model have revealed no consistent difference in fast synaptic calcium entry (31,32) or reduced metabotropic glutamate receptor (mGluR)-dependent calcium entry (33), making it unlikely that changes in activation of conventional PKC isozymes by Ca^{2+} could explain the observed increases in PKC activity. Importantly, activation of conventional PKC isozymes requires binding by both Ca^{2+} and diacylglycerol (DAG) (34). We investigated expression of key enzymes for DAG metabolism and identified reduced expression of *Dagla* (Fig. 2F) (wild type 5 weeks: 1.02 ± 0.12, ATXN1[82Q]$^{tg/tg}$ 5 weeks: 0.37 ± 0.07, wild type 15 weeks: 1.04 ± 0.10, ATXN1[82Q]$^{tg/tg}$ 15 weeks: 0.32 ± 0.11). *Dagla* encodes DAG lipase alpha, which metabolizes DAG, and blocking DAG lipase function has been shown to prolong activation of PKCα in Purkinje neurons (35), suggesting that the observed increase in PKC substrate phosphorylation in ATXN1[82Q]$^{tg/tg}$ Purkinje neurons could be explained by increased PKC activity secondary to reduced *Dagla* expression.

Increased PKC activity is a protective modifier of Purkinje neuron degeneration in SCA1 mice

To assess the significance of increased PKC activity for neurodegeneration in SCA1 Purkinje neurons, we inhibited PKC activity in ATXN1[82Q] mice and assessed the effect on Purkinje neuron pathology. PKC activity was inhibited in ATXN1[82Q]$^{tg/-}$ mice by intercrossing with PKCi$^{tg/-}$ mice that express a pseudosubstrate PKC inhibitor peptide under the control of the Purkinje neuron-specific L7/Pcp2 promoter (36). As expression of both the PKCi transgene and ATXN1[82Q] transgene is limited to Purkinje neurons, this strategy allows for evaluation of the cell-autonomous role for increased PKC activity in Purkinje neuron degeneration. ATXN1[82Q]$^{tg/-}$; PKCi$^{tg/-}$ mice showed a reduction of cerebellar PKC substrate phosphorylation relative to ATXN1[82Q]$^{tg/-}$ mice (Fig. 3A) (wild type: 1.00 ± 0.03 AU, PKCi$^{tg/-}$: 1.00 ± 0.19 AU, ATXN1[82Q]$^{tg/-}$: 1.32 ± 0.11 AU, ATXN1[82Q]$^{tg/-}$; PKCi$^{tg/-}$: 1.06 ± 0.05 AU. N = 6 for each group).

Notably, assessment of Purkinje neuron pathology revealed accelerated Purkinje neuron degeneration in ATXN1[82Q]$^{tg/-}$; PKCi$^{tg/-}$ mice. Molecular layer thickness, a measure of Purkinje neuron dendrite integrity, was significantly decreased in ATXN1[82Q]$^{tg/-}$; PKCi$^{tg/-}$ mice compared to both wild-type and PKCi$^{tg/-}$ mice at a time point where molecular layer thickness changes are not yet detected in ATXN1[82Q]$^{tg/-}$ mice (Fig. 3B and D). The accelerated neurodegeneration in ATXN1[82Q]$^{tg/-}$; PKCi$^{tg/-}$ mice was also confirmed with whole-cell capacitance measurements, which revealed that the severity of Purkinje neuron atrophy was significantly greater in ATXN1[82Q]$^{tg/-}$; PKCi$^{tg/-}$ mice compared to ATXN1[82Q]$^{tg/-}$ mice (Fig. 3C). These data suggest that the increased PKC activity observed in SCA1 mice is a protective modifier of neurodegeneration.

Increased PKC activity is a shared protective modifier pathway in other ataxias

To explore a potential role for PKC enzymes in another cerebellar ataxia, we examined whether PKC activity was altered in a mouse model of SCA2 (37). In this model of SCA2, glutamine-expanded ATXN2 is expressed solely in cerebellar Purkinje neurons (38). Similar to ATXN1[82Q]$^{tg/tg}$ mice, whole cerebellar extracts from ATXN2[127Q]$^{tg/-}$ mice (38) exhibited a significant increase in phosphorylation of PKC substrates (Fig. 4A and B) (wild type: 1.00 ± 0.07 AU, ATXN2[127Q]$^{tg/-}$: 1.21 ± 0.07 AU). ATXN2[127Q]$^{tg/-}$ cerebella also showed reduced *Dagla* transcript levels (Fig. 4C) (wild type: 1.01 ± 0.04, ATXN2[127Q]$^{tg/-}$: 0.55 ± 0.12), suggesting that reduced *Dagla* expression could be a shared mechanism for increased PKC activity in SCA1 and SCA2 mice. Moreover, prior work has also suggested that mutant Atxn2 directly facilitates calcium release from intracellular stores important for PKC activation (39). We crossed ATXN2[127Q]$^{tg/-}$ mice with PKCi$^{tg/-}$ mice to generate ATXN2[127Q]$^{tg/-}$; PKCi$^{tg/-}$ progeny. ATXN2[127Q]$^{tg/-}$; PKCi$^{tg/-}$ mice showed a reduction of PKC substrate phosphorylation relative to ATXN2[127Q]$^{tg/-}$ mice (Fig. 4D) (wild type: 1.00 ± 0.17 AU, PKCi$^{tg/-}$: 1.05 ± 0.36 AU, ATXN2[127Q]$^{tg/-}$: 1.37 ± 0.03 AU, ATXN2[127Q]$^{tg/-}$; PKCi$^{tg/-}$: 1.24 ± 0.021 AU. N = 4 for each group). At 25 weeks, ATXN2[127Q]$^{tg/-}$; PKCi$^{tg/-}$ mice showed significantly greater thinning of the molecular layer in the intermediate zone relative to litter-mate ATXN2[127Q]$^{tg/-}$ mice (Fig. 4E and F). These data demonstrate that increases in PKC activity oppose dendritic degeneration in several models of ataxia.

To further explore the spectrum of cerebellar disease in which PKC activity may modify disease pathogenesis, we examined human post-mortem tissue of MSA, a sporadic, heterogeneous neurodegenerative disease that in some cases can have prominent Purkinje neuron loss (40). We assessed PKC substrate phosphorylation in surviving Purkinje neurons from post-mortem MSA samples that were noted at autopsy to have significant Purkinje neuron loss (demographics summarized in Supplementary Material, Table S2). MSA samples were compared to age-matched samples from patients with Alzheimer disease (AD), a neurodegenerative disease with limited cerebellar involvement (41,42). AD tissue was used as a control in order to determine whether merely having a neurodegenerative disease was sufficient to increase PKC substrate phosphorylation. MSA Purkinje neurons showed a significant increase in phosphorylated PKC substrate-to-calbindin ratio relative to age-matched AD controls (Supplementary Material, Fig. S3A and B) (AD: 0.71 AU, MSA: 1.63 AU). Calbindin levels (AD: 1383.52 AU, MSA: 1076.80 AU) and absolute staining intensity for phosphorylated PKC substrates (AD: 919.74 AU, MSA: 1072.13 AU) were not, however, significantly different between the two groups (Supplementary Material, Fig. S3C and D). Although it is possible that a partial reduction in calbindin levels may explain the apparent increase in PKC activity in MSA, PKC activity may be a modulator of neuropathology in both dominantly inherited ataxias, and in other neurodegenerative ataxias with Purkinje neuron involvement.

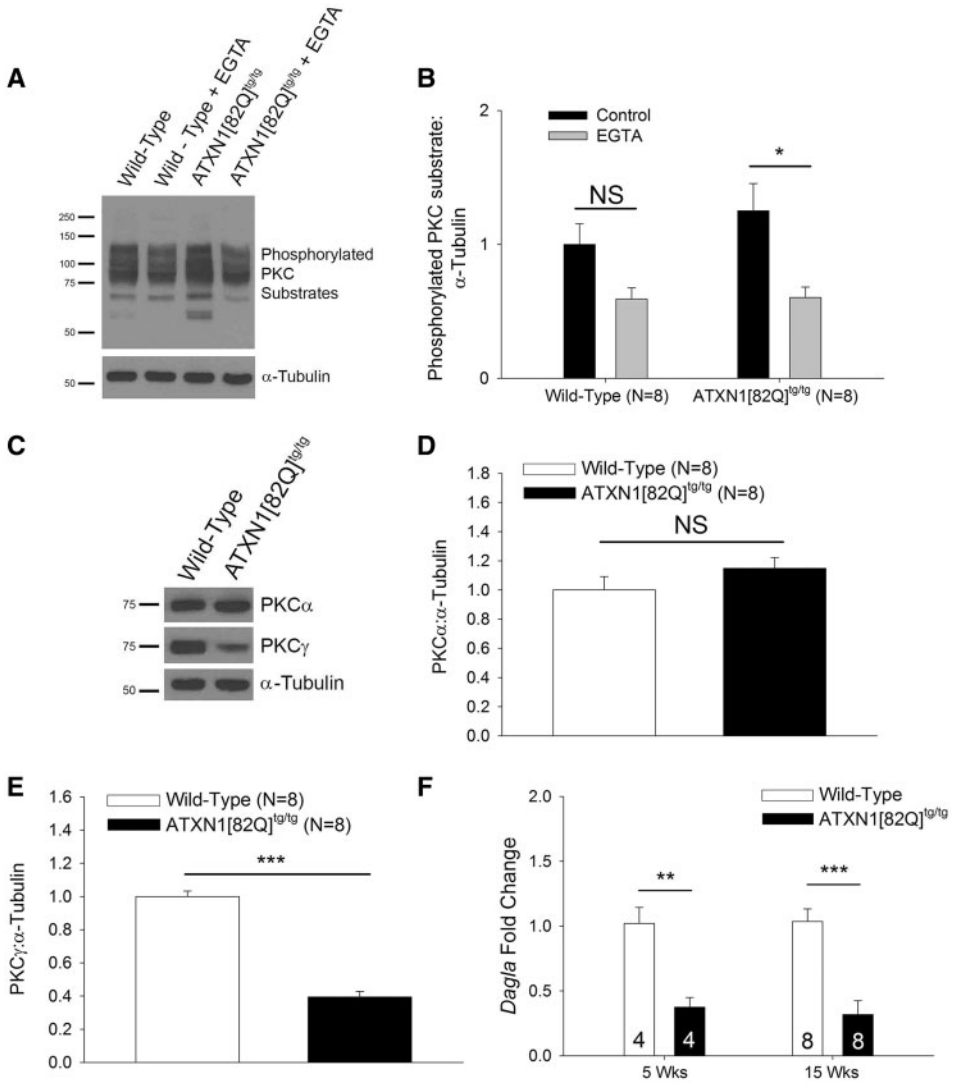

Figure 2. Increased PKC substrate phosphorylation is mediated by conventional PKC isozymes in SCA1. (**A**) Representative western blot for phosphorylated PKC substrates in organotypic cerebellar slice cultures treated with 5 mM EGTA from 15-week-old mice. Calcium chelation with EGTA reduced PKC substrate phosphorylation in ATXN1[82Q]$^{tg/tg}$ slice cultures but not wild-type slice cultures, summarized in (**B**). Tubulin was used as a loading control. (**C**) Representative western blot for PKCα and PKCγ in 15-week-old mice. Unchanged expression of PKCα in ATXN1[82Q]$^{tg/tg}$ cerebella at 15 weeks of age is summarized in (**D**), while reduced expression of PKCγ in ATXN1[82Q]$^{tg/tg}$ cerebella at 15 weeks of age is summarized in (**E**). Tubulin was used as a loading control. (**F**) *Dagla* transcripts are reduced at 5 and 15 weeks in ATXN1[82Q]$^{tg/tg}$ cerebella as assessed using quantitative RT-PCR. Number of animals from each group indicated within bars. Throughout, data are represented as means with error bars representing S.E.M. NS = not significant; * $P < 0.05$; ** $P < 0.01$; *** $P < 0.001$. Statistical significance derived by two-way ANOVA (B) or unpaired two-tailed Student's *t*-test (D, E, F).

Increased PKC activity limits Purkinje neuron excitability in ataxia

Previous studies have demonstrated that altered intrinsic excitability is an important driver of neurodegeneration in the ATXN1[82Q] model of SCA1 (20,23) and in other models of cerebellar ataxia (43,44). Altered Purkinje neuron spiking is also described in cerebellar slices from mouse models of SCA2 (38), SCA3 (45) and SCA6 (46) as well as *in vivo* in SCA2 mice (47). PKC family members influence the function of ion channels that regulate membrane excitability (18,48–50), and we therefore sought to investigate whether increased PKC activity might exert its neuroprotective effect by altering Purkinje neuron excitability.

To assess this possibility, cell-attached and whole-cell patch clamp somatic recordings were performed from ATXN1[82Q]$^{tg/-}$; PKCi$^{tg/-}$ and litter-mate control Purkinje neurons in acute cerebellar slices at 20 weeks of age. Baseline firing properties were abnormal in both ATXN1[82Q]$^{tg/-}$; PKCi$^{tg/-}$ mice and ATXN1[82Q]$^{tg/-}$ mice as compared to litter-mate wild-type and PKCi$^{tg/-}$ controls (Fig. 5A). Both ATXN1[82Q]$^{tg/-}$ and ATXN1[82Q]$^{tg/-}$; PKCi$^{tg/-}$ Purkinje neurons exhibited reduction in firing frequency (Fig. 5B) and increased spike irregularity (Fig. 5C). Analysis of spikes from whole-cell patch clamp recordings of baseline spiking revealed reduced amplitude (Fig. 5D and E) of the after-hyperpolarization (AHP), consistent with our prior work in this model of SCA1 (23). This reduction in the AHP likely underlies the irregular spiking (51,52). Importantly, these spiking parameters were similarly altered in both ATXN1[82Q]$^{tg/-}$ and ATXN1[82Q]$^{tg/-}$; PKCi$^{tg/-}$ Purkinje neurons.

In contrast to the similarity in basal spiking between ATXN1[82Q]$^{tg/-}$ and ATXN1[82Q]$^{tg/-}$; PKCi$^{tg/-}$ Purkinje neurons, ATXN1[82Q]$^{tg/-}$; PKCi$^{tg/-}$ Purkinje neurons were hyperexcitable relative to ATXN1[82Q]$^{tg/-}$ Purkinje neurons in response to

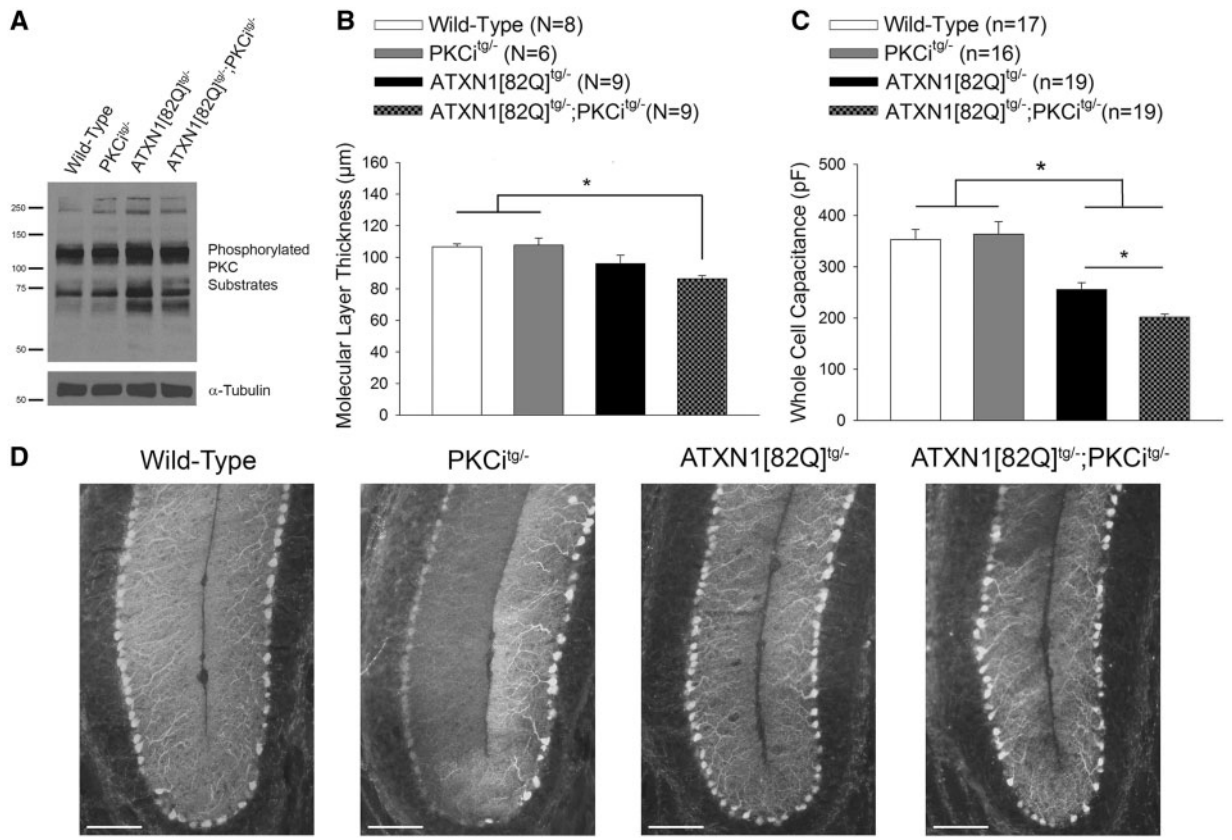

Figure 3. Increased PKC substrate phosphorylation is a protective modifier of neurodegeneration in SCA1 mice. (**A**) Representative western blot for PKC substrate phosphorylation in wild-type, PKCi$^{tg/-}$, ATXN1[82Q]$^{tg/-}$ and ATXN1[82Q]$^{tg/-}$; PKCi$^{tg/-}$ mice at 20 weeks of age demonstrating reduction of PKC substrate phosphorylation in ATXN1[82Q]$^{tg/-}$; PKCi$^{tg/-}$ mice. Tubulin was used as a loading control. (**B**) Reduced molecular layer thickness in lobule V of ATXN1[82Q]$^{tg/-}$; PKCi$^{tg/-}$ mice at 20 weeks of age. (**C**) Whole-cell capacitance measurements in ATXN1[82Q]$^{tg/-}$; PKCi$^{tg/-}$ Purkinje neurons from the anterior cerebellar vermis show a greater reduction in cell size relative to ATXN1[82Q]$^{tg/-}$ Purkinje neurons, which are atrophied relative to wild-type and PKCi$^{tg/-}$ Purkinje neurons at 20 weeks of age. (**D**) Representative images at the cerebellar primary fissure in wild-type, PKCi$^{tg/-}$, ATXN1[82Q]$^{tg/-}$ and ATXN1[82Q]$^{tg/-}$; PKCi$^{tg/-}$ mice stained with calbindin at 20 weeks of age. Scale bar, 100 μm. Throughout, data are represented as means with error bars representing S.E.M. * $P<0.05$. Statistical significance derived by one-way ANOVA with Holm-Sidak multiple comparison test (B, C).

injected current. ATXN1[82Q]$^{tg/-}$; PKCi$^{tg/-}$ Purkinje neurons could not sustain spiking in response to depolarizing current injection to the same level as ATXN1[82Q]$^{tg/-}$ Purkinje neurons (Fig. 6A and B). This abnormality occurred despite a similar input resistance for ATXN1[82Q]$^{tg/-}$; PKCi$^{tg/-}$ Purkinje neurons and ATXN1[82Q]$^{tg/-}$ Purkinje neurons (Supplementary Material, Fig. S4A). This increase in excitability caused by PKCi transgene expression was restricted to the SCA1 background, as the threshold for depolarization block was indistinguishable between PKCi$^{tg/-}$ and wild-type mice (Supplementary Material, Fig. S4B). Hyperexcitability in response to injected current has been observed previously in this model of SCA1 (23), and has also been observed in Purkinje neurons from other models of ataxia (45,53). This suggests that PKC activity suppresses pathologic changes in Purkinje neuron excitability that are observed across multiple models of ataxia.

In addition to action potentials originating at the axon initial segment, Purkinje neurons demonstrate dendritic spikes mediated by voltage-gated calcium channels (54). A reduced threshold to dendritic calcium spikes in response to current injection reflects an increased intrinsic dendritic membrane excitability (55). Dendritic excitability is perturbed in the ATXN1[82Q] model of SCA1, and targeting increased dendritic membrane excitability has been found to be an effective therapeutic strategy in this model (56). To assess whether PKC activity modulates dendritic excitability, we examined whether the threshold to elicit dendritic calcium spikes in response to somatic current injection (in the presence of tetrodotoxin to block action potentials originating at the axon initial segment) differed between ATXN1[82Q]$^{tg/-}$ and ATXN1[82Q]$^{tg/-}$; PKCi$^{tg/-}$ Purkinje neurons. Indeed, ATXN1[82Q]$^{tg/-}$; PKCi$^{tg/-}$ Purkinje neurons required less injected current to elicit dendritic calcium spikes (Fig. 6C and D) in the absence of changes in input resistance (Supplementary Material, Fig. S4C). This finding suggests that dendritic excitability is increased in ATXN1[82Q]$^{tg/-}$; PKCi$^{tg/-}$ Purkinje neurons.

Importantly, structural changes in the dendritic arbor by themselves would be predicted to produce changes in the electrical properties of the dendrites (57), raising the possibility that the observed differences in dendritic excitability between ATXN1[82Q]$^{tg/-}$ and ATXN1[82Q]$^{tg/-}$; PKCi$^{tg/-}$ Purkinje neurons could be explained by accelerated dendritic degeneration rather than PKC inhibition in ATXN1[82Q]$^{tg/-}$; PKCi$^{tg/-}$ mice. To explore this possibility, dendritic calcium spike threshold was assessed in ATXN1[82Q]$^{tg/-}$ Purkinje neurons from acute cerebellar slices where PKC substrate phosphorylation was suppressed with the PKC inhibitor Go6983. Go6983 lowered dendritic calcium spike threshold (Fig. 6E) in the absence of changes in input resistance (Supplementary Material, Fig. S4D). Taken together, these findings demonstrate that increased PKC activity in ATXN1[82Q]$^{tg/-}$ Purkinje neurons suppresses dendritic excitability.

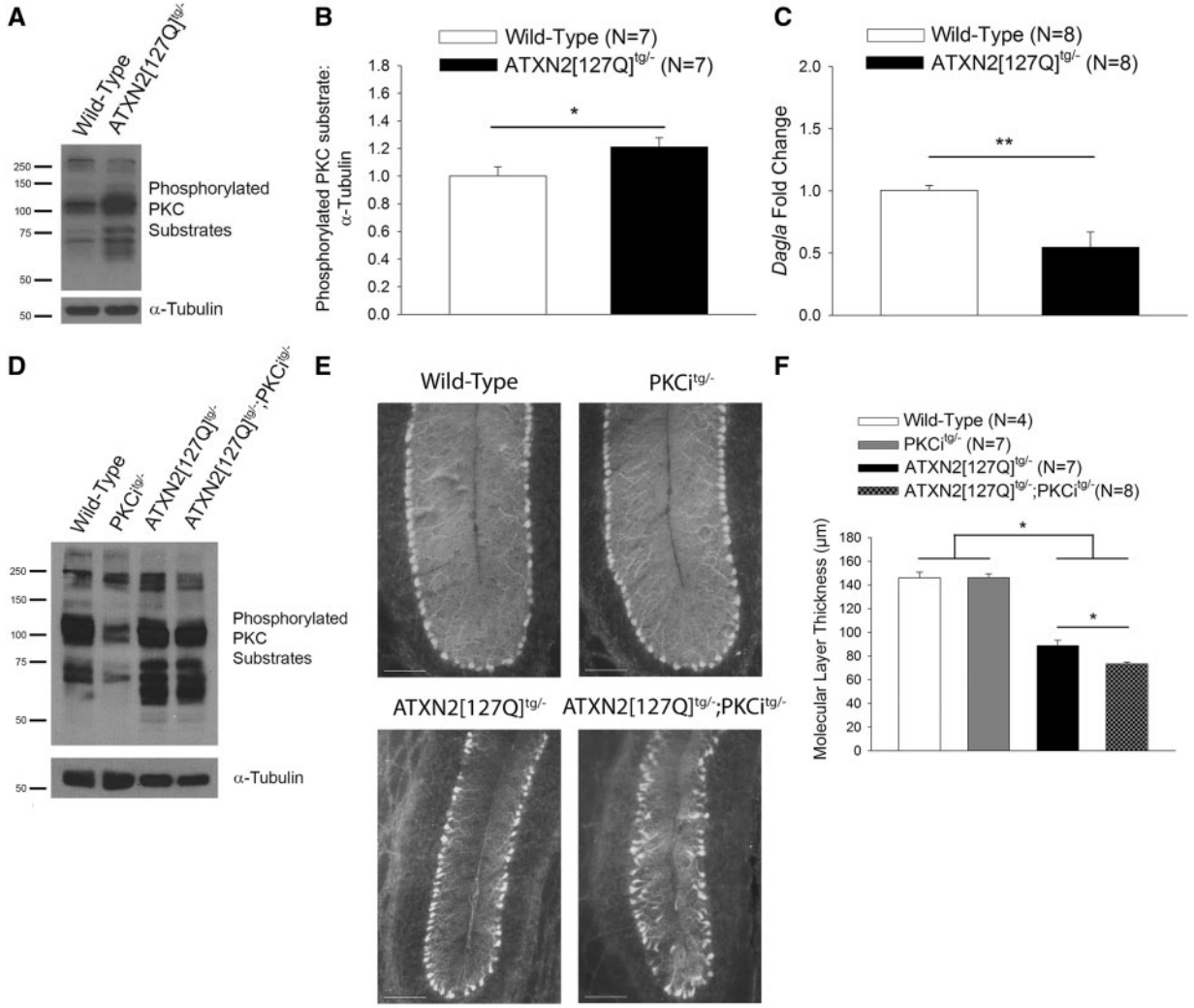

Figure 4. Increased PKC substrate phosphorylation is a shared protective pathway in SCA2 mice. (**A**) Representative western blot for PKC substrate phosphorylation in wild-type and ATXN2[127Q]$^{tg/-}$ cerebella at 12 weeks of age demonstrating increased PKC substrate phosphorylation, summarized in (**B**). Tubulin was used as a loading control. (**C**) Expression of *Dagla* is reduced at 12 weeks in ATXN2[127Q]$^{tg/-}$ cerebella as assessed using quantitative RT-PCR. (**D**) Representative western blot for PKC substrate phosphorylation in wild-type, PKCi$^{tg/-}$, ATXN2[127Q]$^{tg/-}$ and ATXN2[127Q]$^{tg/-}$; PKCi$^{tg/-}$ mice at 25 weeks of age demonstrating reduction of PKC substrate phosphorylation in ATXN2[127Q]$^{tg/-}$; PKCi$^{tg/-}$ mice. Tubulin was used as a loading control. (**E**) Representative images at the cerebellar primary fissure in sections from wild-type, PKCi$^{tg/-}$, ATXN2[127Q]$^{tg/-}$ and ATXN2[127Q]$^{tg/-}$; PKCi$^{tg/-}$ mice stained with calbindin at 25 weeks of age. Scale bar, 100 μm. (**F**) Reduced molecular layer thickness in lobule VI of ATXN2[127Q]$^{tg/-}$; PKCi$^{tg/-}$ mice at 25 weeks of age. Throughout, data are represented as means with error bars representing S.E.M. NS = not significant; * $P < 0.05$; ** $P < 0.01$. Statistical significance derived by unpaired two-tailed Student's *t*-test (B, C) or one-way ANOVA with Holm-Sidak multiple comparison test (F).

If PKC substrate phosphorylation were exerting its neuroprotective effect by limiting Purkinje neuron excitability, then altered membrane excitability should be observed when PKC activity is modulated in the ATXN2[127Q] model of SCA2. As with ATXN1[82Q]$^{tg/-}$; PKCi$^{tg/-}$ Purkinje neurons, ATXN2[127Q]$^{tg/-}$; PKCi$^{tg/-}$ Purkinje neurons require less injected current to elicit dendritic calcium spikes relative to ATXN2[127Q]$^{tg/-}$ Purkinje neurons (Fig. 6F) in the absence of changes in input resistance (Supplementary Material, Fig. S4E). Together with the findings from the SCA1 model these data suggest that conventional PKC isozymes may be mediating their protective effect on Purkinje neuron degeneration by limiting membrane hyperexcitability.

Discussion

In the current study, we demonstrate that increased PKC activity within Purkinje neurons is observed in mouse models of ataxia and human post-mortem SCA1 tissue. While the mechanism for increased PKC activity remains unclear, we have observed a reduction in *Dagla* transcripts in SCA1 and SCA2 mice that accompanies and may play a role in increased PKC activation. We also demonstrate in mouse models of both SCA1 and SCA2 that the increased PKC activity is a protective modifier of neurodegeneration. The worsened neurodegeneration following normalization of PKC activity in these ataxia models does not represent a non-specific deleterious effect of overexpression of two different transgenes in Purkinje neurons. Inhibiting a different kinase, Akt, through overexpression of a dominant negative Akt in Purkinje neurons of ATXN1[82] mice does not worsen Purkinje neuron degeneration (58). Increased membrane excitability is a known driver of Purkinje neuron degeneration in mouse models of SCA1 and SCA2, and we find that PKC activity reduces membrane excitability in these models, suggesting that PKC activity may exert its neuroprotective effect on

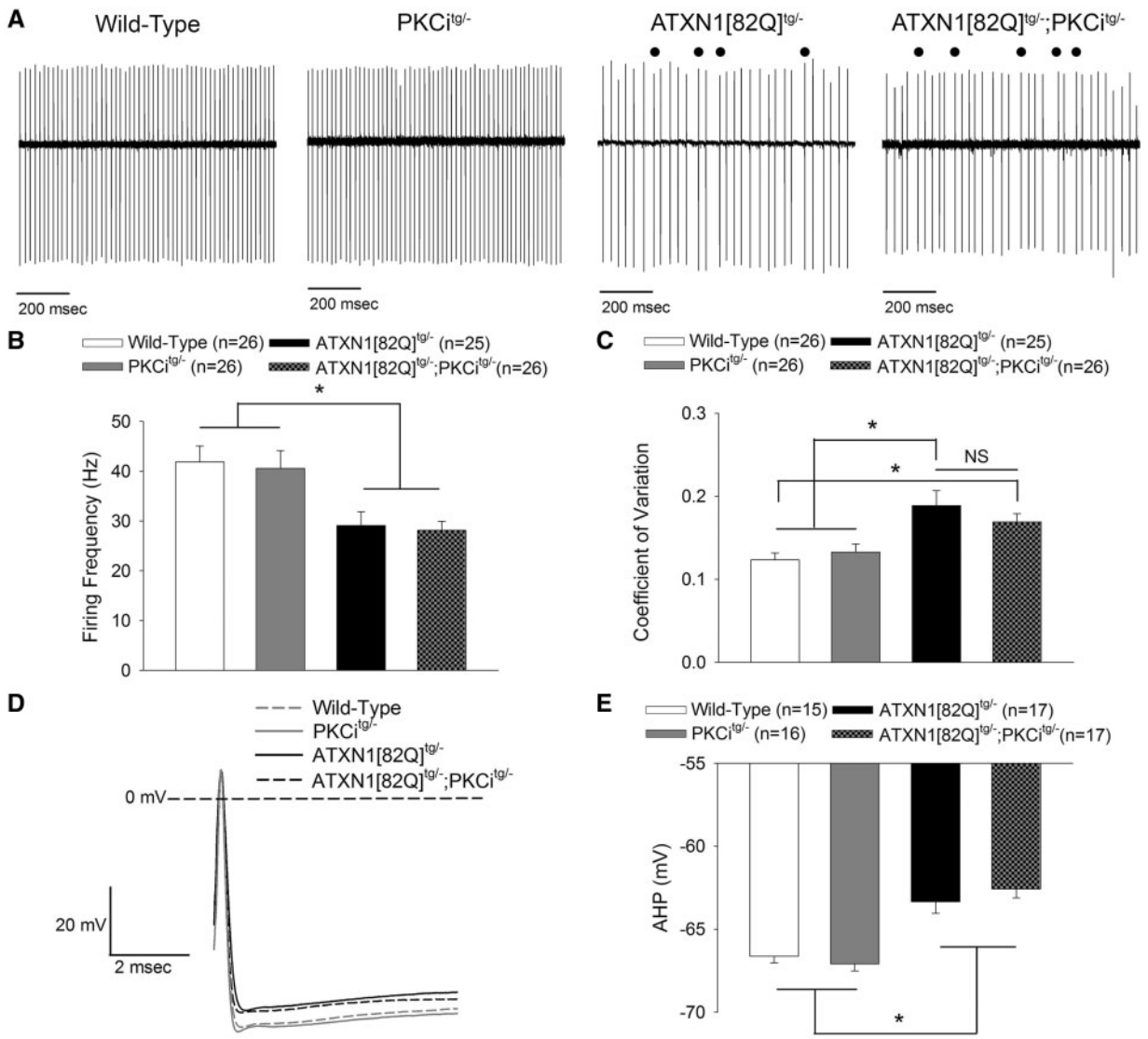

Figure 5. The increase in PKC activity in SCA1 mice is not associated with alterations in Purkinje neuron spiking. (**A**) Representative firing from wild-type, PKCi$^{tg/-}$, ATXN1[82Q]$^{tg/-}$ and ATXN1[82Q]$^{tg/-;}$ PKCi$^{tg/-}$ Purkinje neurons. ATXN1[82Q]$^{tg/-}$ and ATXN1[82Q]$^{tg/-;}$ PKCi$^{tg/-}$ mice show irregular spiking, with abnormal pauses marked. (**B**) ATXN1[82Q]$^{tg/-}$ and ATXN1[82Q]$^{tg/-}$; PKCi$^{tg/-}$ Purkinje neurons show reduced firing frequency. (**C**) ATXN1[82Q]$^{tg/-}$ and ATXN1[82Q]$^{tg/-}$; PKCi$^{tg/-}$ Purkinje neurons show more irregular firing, indicated by a higher CV. (**D**) Representative spontaneous action potentials from wild-type, PKCi$^{tg/-}$, ATXN1[82Q]$^{tg/-}$ and ATXN1[82Q]$^{tg/-}$; PKCi$^{tg/-}$ Purkinje neurons. ATXN1[82Q]$^{tg/-}$ and ATXN1[82Q]$^{tg/-}$; PKCi$^{tg/-}$ Purkinje neurons have an AHP which does not achieve the same degree of hyperpolarization as wild-type and PKCi Purkinje neurons, summarized in (**E**). Throughout, data are represented as means with error bars representing S.E.M. NS = not significant; * $P < 0.05$. Statistical significance derived by one-way ANOVA with Holm-Sidak multiple comparison test (B, C, E).

Purkinje neurons through its role as a regulator of ion channel function.

Purkinje neuron PKC activation is required for long-term depression (LTD) at the parallel fiber-to-Purkinje neuron synapse (36), and it is also required for the suppression in Purkinje neuron intrinsic excitability that accompanies this form of LTD (59). PKC activation thus suppresses glutamatergic synaptic transmission and intrinsic excitability in Purkinje neurons. Notably, introducing a phosphomimetic mutation of Ser^{880} on GluA2 occludes LTD at the parallel fiber synapse (60). Also, ATXN1[82Q] transgenic mice are unable to induce parallel fiber LTD after 5 weeks of age (33), such that our finding of increased Ser^{880} GluA2 phosphorylation in ATXN1[82Q] mice due to increased PKC activity may contribute to disease-associated changes in synaptic transmission. We also observed that inhibiting PKC activity increases intrinsic excitability in both ATXN1[82Q] and ATXN2[127Q] mice, suggesting that increased PKC activity modulates intrinsic excitability in SCA1 and SCA2. Our findings therefore suggest a role for increased PKC activity in both altered synaptic function and intrinsic membrane excitability in cerebellar ataxia.

Changes in Purkinje neuron intrinsic excitability are widespread in models of ataxia (23,51–53,61–63). Altered Purkinje neuron spiking is a consistent feature in a number of mouse models of ataxia. In mouse models of SCA1, SCA2 and SCA3 at early stages of disease, increased membrane excitability results in membrane depolarization and a lack of spiking (23,45,53,56) attributed to depolarization block. At different disease stages, a reduction in Purkinje neuron firing frequency is consistently seen in models of SCA1 (20,23), SCA2 (38,53), and SCA6 (46) *in vitro*, often in association with irregular spiking *in vitro* and *in vivo* (46,47,61). These aberrant patterns of firing are also present in

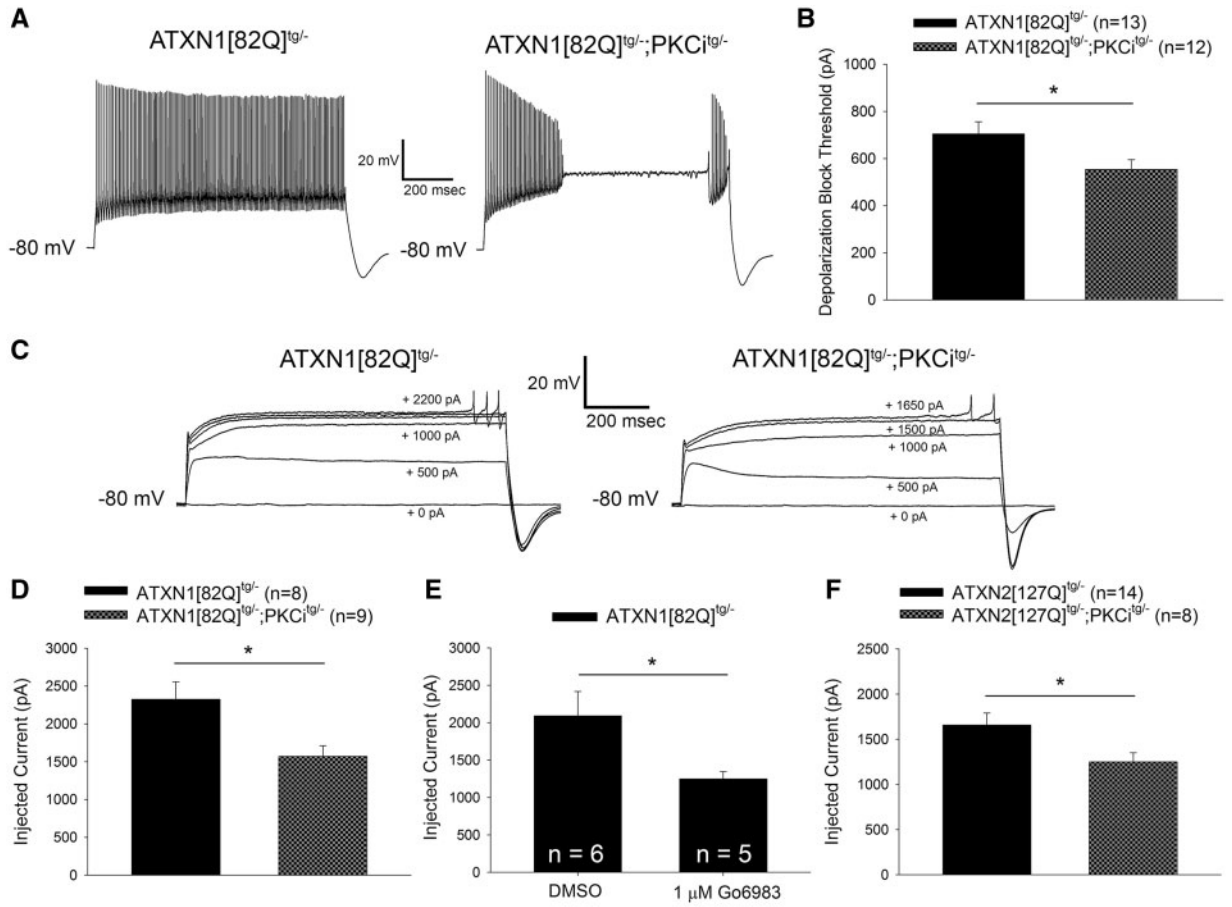

Figure 6. Increased PKC activity reduces membrane excitability in SCA1 and SCA2 Purkinje neurons. (**A**) Representative traces from ATXN1[82Q]$^{tg/-}$ and ATXN1[82Q]$^{tg/-}$; PKCi$^{tg/-}$ Purkinje neurons injected with +700 pA of current. ATXN1[82Q]$^{tg/-}$; PKCi$^{tg/-}$ Purkinje neurons undergo depolarization block of repetitive spiking at lower levels of injected current than ATXN1[82Q]$^{tg/-}$ Purkinje neurons, summarized in (**B**). (**C**) Representative traces where dendritic calcium spikes were evoked with somatic current injection (injected current amount indicated on the trace) from ATXN1[82Q]$^{tg/-}$ (left) and ATXN1[82Q]$^{tg/-}$; PKCi$^{tg/-}$ (right) Purkinje neurons treated with 1 μm TTX. ATXN1[82Q]$^{tg/-}$; PKCi$^{tg/-}$ Purkinje neurons require less injected current to elicit a dendritic calcium spike than ATXN1[82Q]$^{tg/-}$ Purkinje neurons, summarized in (**D**). (**E**) ATXN1[82Q]$^{tg/-}$ Purkinje neurons require less injected current to elicit a dendritic calcium spike in the presence of 1 μM TTX when PKC activity is inhibited with 1 μM Go6983. All slices were pre-incubated with dimethyl sulfoxide (DMSO) or Go6983 for 40 min before recording. (**F**) ATXN2[127Q]$^{tg/-}$; PKCi$^{tg/-}$ Purkinje neurons require less injected current to elicit a dendritic calcium spike in the presence of 1 μM TTX than ATXN2[127Q]$^{tg/-}$ Purkinje neurons. All data from experiments using ATXN1[82Q]$^{tg/-}$; PKCi$^{tg/-}$ were performed at 20 weeks of age, when dendritic degeneration is detected in these mice. All data from experiments using ATXN2[127Q]$^{tg/-}$; PKCi$^{tg/-}$ were performed at 12 weeks of age, when dendritic degeneration is first detected in ATXN2[127Q]$^{tg/-}$ mice (38). Throughout, data are represented as means with error bars representing S.E.M. * $P < 0.05$. Statistical significance derived by unpaired two-tailed Student's *t*-test (B, D, E, F).

mouse models of ataxia resulting from calcium channel mutations (51,52,64). Notably, studies of Purkinje neuron membrane excitability in models of SCA1 (23) and SCA2 (43) have revealed that increased excitability also drives Purkinje neuron degeneration. In these studies, activation of potassium channels reduces excitability and prevents Purkinje neuron degeneration; in the present study, increased excitability secondary to reduced PKC activity is observed in association with accelerated degeneration. While other roles for PKC could explain its neuroprotective role in SCA1 and SCA2 mice, the established role for increased excitability as a driver of degeneration in these models makes a compelling case for PKC acting through pathways that influence membrane excitability to modify pathology in SCA1 and SCA2. The findings from this study add further support to the critical role for increased intrinsic membrane excitability in Purkinje neuron degeneration in SCA1 and SCA2.

Phosphorylation by PKC modulates the peak current (48,65,66), voltage dependence (67,68) or kinetics (18,69) of a diverse array of channels that includes voltage-gated sodium channels, voltage-gated calcium channels, potassium channels and non-selective cation channels. There are, therefore, many possible ion channel targets through which PKC activity could reduce Purkinje neuron excitability in SCA1 and SCA2. An ion channel targeted by PKC that is very relevant to the findings of the present study is $K_v3.3$, which shows slowed inactivation upon phosphorylation by PKC (18). Mutations in *KCNC3* (encoding $K_v3.3$) result in spinocerebellar ataxia type 13 (SCA13) (70) and most SCA13 mutations result in impaired channel function (71). Furthermore, Purkinje neurons from mice lacking *Kcnc3* expression show an increased propensity for dendritic calcium spikes (55), which is similar to what was observed in the present study. These findings suggest that the potentiation of $K_v3.3$ by PKC isozymes may be particularly important for explaining reduced excitability and neuroprotection in SCA1 and SCA2. Future studies could evaluate the effects of increased PKC activity on individual ion channel targets, including $K_v3.3$.

The findings from the present study may be relevant to understanding disease pathogenesis in not only SCA1, SCA2 and

possibly MSA, but also in SCA14. Various mutations in *PRKCG* have been described for SCA14, but the mechanisms by which mutant PKCγ produces Purkinje neuron degeneration remain unclear. Increased kinase function (13), impaired kinase function (16) and protein misfolding (14) have all been proposed as possible mechanisms of disease. There is evidence that SCA14 mutations produce PKCγ with increased *in vitro* kinase activity and membrane targeting (72), but mutant PKCγ also has a reduced capacity to phosphorylate ion channel targets (16) and exerts a dominant-negative effect on PKCα (15). The findings from the present study support the conclusion that PKC activity supports Purkinje neuron health, which is most consistent with a loss-of-function mechanism in SCA14. Furthermore, the present study suggests that increased Purkinje neuron excitability may play a meaningful role in the pathogenesis of SCA14. It is therefore important to examine intrinsic membrane excitability in models of SCA14.

Materials and Methods

Mice

All animal procedures were approved by the University of Michigan Committee on the Use and Care of Animals. ATXN1[82Q] transgenic mice (73) overexpress mutant human ATXN1 with 82 CAG repeats selectively in cerebellar Purkinje neurons under the Purkinje neuron-specific murine *Pcp2 (L7)* promoter and were maintained on an FVB background (Jackson Labs). ATXN1[82Q]$^{tg/tg}$ mice were maintained homozygous for the transgene (23) except as indicated below. ATXN1[82Q]$^{tg/tg}$ mice were used between 5 and 15 weeks old. Age- and sex-matched wild-type FVB mice were used as controls for these studies. The ATXN2[127Q]$^{tg/-}$ transgenic mice (38) overexpress mutant human ATXN2 with 127 CAG repeats selectively in cerebellar Purkinje neurons under the *Pcp2 (L7)* promoter and were maintained on a mixed background. These mice were generated on a B6D2F1 hybrid background (Jackson Labs) and the line was maintained by crossing to this hybrid strain. Experiments using ATXN2[127Q] mice were done using hemizygous ATXN2[127Q]$^{tg/-}$ mice compared to wild-type ATXN2[127Q]$^{-/-}$ litter-mate controls. Mice used for these experiments were 12 weeks old. PKCi$^{tg/-}$ mice (36) express the pseudosubstrate PKC inhibitor (PKCi) peptide selectively in Purkinje neurons under the *Pcp2 (L7)* promoter and were maintained on a C57B6J background (Jackson Labs). A balance of mice of both sexes were used in all studies.

In all experiments where ATXN1[82Q]$^{tg/-}$; PKCi$^{tg/-}$ mice were used, animals were always compared to litter-mate controls. Experimental mice originated from crosses between ATXN1[82Q]$^{tg/-}$ mice on an FVB background and PKCi$^{tg/-}$ mice on a C57B6J background, such that all experimental animals were F1 hybrids. The genotypes of mice used are specified as follows:

Wild type: ATXN1[82Q]$^{-/-}$; PKCi$^{-/-}$

PKCi$^{tg/-}$: ATXN1[82Q]$^{-/-}$; PKCi$^{tg/-}$

ATXN1[82Q]$^{tg/-}$: ATXN1[82Q]$^{tg/-}$; PKCi$^{-/-}$

ATXN1[82Q]$^{tg/-}$; PKCi$^{tg/-}$: ATXN1[82Q]$^{tg/-}$; PKCi$^{tg/-}$

All data presented from these experiments were from mice at 20 weeks of age.

In all experiments where ATXN2[127Q]$^{tg/-}$; PKCi$^{tg/-}$ mice were used, animals were always compared to litter-mate controls. Experimental mice originated from crosses between ATXN2[127Q]$^{tg/-}$ mice on a B6D2F1 hybrid background and PKCi$^{tg/-}$ mice on a C57B6J background. The genotypes of mice used are specified as follows:

Wild type: ATXN2[127Q]$^{-/-}$; PKCi$^{-/-}$

PKCi$^{tg/-}$: ATXN2[127Q]$^{-/-}$; PKCi$^{tg/-}$

ATXN2[127Q]$^{tg/-}$: ATXN2[127Q]$^{tg/-}$; PKCi$^{-/-}$

ATXN2[127Q]$^{tg/-}$; PKCi$^{tg/-}$: ATXN2[127Q]$^{tg/-}$; PKCi$^{tg/-}$

All data presented from these experiments were from mice at either 12 or 25 weeks of age.

Western blotting

Preparation of whole cerebellar samples

Mice were euthanized following anesthesia with isoflurane, and cerebella were removed and flash -frozen in liquid nitrogen. Tissue was stored at −80°C until the time of processing.

Igepal homogenization buffer was prepared as follows: 50 mM Tris–HCl, 150 mM NaCl, 5 mM EDTA, 1 mM EGTA, pH to 8.0, 1% Igepal CA-630 (cat. no. I8896, Sigma-Aldrich). EDTA-free protease inhibitor tablets (cat. no. 11873580001, Sigma-Aldrich) and PhosSTOP phosphatase inhibitor tablets (cat. no. 4906845001, Sigma-Aldrich) were added to homogenization buffer immediately before use. Whole cerebellar samples were homogenized using a Potter-Helvejm tissue grinder (Corning). The supernatants (soluble protein fractions) were collected and total protein concentration was determined using the Pierce BCA protein assay kit (prod. no. 23225, ThermoFisher), at which point the supernatants were resuspended in Laemmli buffer. Samples were then utilized immediately for western blots.

Preparation of organotypic slice culture samples

Sagittal brain slices (300 μm thickness) were prepared as reported previously (23). A total of 5–6 slices per brain were used in each set of cultures, divided evenly between control medium and experimental medium. After a quick wash in the corresponding medium, each slice was placed on a cell culture insert (0.4 μm pore size, 30 mm diameter; Millipore), which had been previously placed on a well (6-well plate) containing 1.2 ml of culture medium that had been pre-incubated at 37°C in 95% O_2/5% CO_2. Control medium was prepared as follows: 50% minimal essential medium with Earle's salts, 25% horse serum, 25% Hank's balanced salts solution, 25 mM HEPES, 2 mM L-glutamine, 6.5 mg/ml glucose. EGTA-containing medium was prepared by starting with control medium, adding EGTA to a final concentration of 5 mM, and adjusting the pH to 7.4 with NaOH. Any slice-culture experiment involving treatment with a pharmacological agent was performed using experimental medium containing the pharmacological agent or control medium which contained an equivalent volume of vehicle.

After 24 h of incubation at 37°C in 95% O_2/5% CO_2, lysates were prepared from cerebellar slices for immunoblotting. For immunoblotting protein lysate preparation, the cerebellum from each brain slice was macrodissected, and all cerebellar samples exposed to a given condition from each mouse were pooled and placed in ice cold Igepal homogenization buffer containing protease and phosphatase inhibitors (40 μl per slice), prepared as described above. Samples were immediately homogenized by pipette trituration followed by sonication in a 500 W sonic dismembranator with Misonix 3″ cup horn attachment (cat. no. FB505110, QSonica). The supernatants (soluble protein fractions) were collected and total protein concentration was determined using the Pierce BCA protein assay kit (prod. no.

23225, ThermoFisher), at which point the supernatants were resuspended in Laemmli buffer. Samples were then utilized immediately for western blots.

In all cases where ATXN1[82Q]$^{tg/tg}$ and wild-type mice were compared, ATXN1[82Q]$^{tg/tg}$ and wild-type mice were matched so that slices were prepared from matched mice on the same day with the same reagents, and all subsequent sample preparation and analysis was performed using matched samples.

Electrophoresis and western blotting. Total protein from whole cerebellar extracts or slice culture extracts (50 μg) were resolved in 8% sodium dodecyl sulfate-polyacrylamide gel electrophoresis (SDS-PAGE) gels. In the case of immunoblots for pSer^{880}-GluA2 in SCA1 mice, 30 μg of wild-type extract and 60 μg of ATXN1[82Q]$^{tg/tg}$ extract were loaded to produce equivalent GluA2 loading, suggesting differences in baseline GluA2 protein levels. After electrophoresis and protein transfer onto a polyvinyl difluoride membrane, corresponding membranes were incubated overnight at 4°C with primary antibodies: rabbit anti-Phospho-(Ser) PKC substrate antibody (1: 1000, Cat. no. 2261, Cell Signaling), rabbit anti-pSer^{880} GluA2 (1: 500, Cat. No. ab52180, Abcam), rabbit anti-GluA2 (1: 10 000, cat. no. ab206293, Abcam), rabbit anti-PKCα (1: 1000, Cat. no. ab4124, Abcam), rabbit anti-PKCγ (1: 2000, Cat. no. ab71558, Abcam), rabbit anti-α-Tubulin (11H10) (1: 5000, Cat. no. 2125, Cell Signaling). Bound primary antibodies were visualized by incubation with a peroxidase-conjugated goat anti-rabbit IgG secondary antibody (1: 10000; Code no. 111-035-003, Jackson ImmunoResearch Laboratories) followed by treatment with the Western Lightning ECL-plus reagent (prod. no. NEL121001EA, PerkinElmer) and exposure to autoradiography films.

Analysis of western blot films

Developed films were scanned and densitometry analysis was performed in ImageJ. For analysis of phosphorylated PKC substrates, the intensity of the entire lane following phospho-(Ser) PKC substrate antibody blotting was normalized to the intensity of α-tubulin band for each mouse. For analysis of pSer^{880}-GluA2, intensity of the pSer^{880}-GluA2 band was normalized to the intensity of total GluA2. For analysis of all other proteins, intensity of the band of interest was normalized to the intensity of α-tubulin for each mouse.

Tissue immunohistochemistry

Paraformaldehyde-fixed mouse immunofluorescence

Mice were anesthetized with isoflurane and brains were removed, fixed in 1% paraformaldehyde for 1 h, immersed in 30% sucrose in PBS and sectioned on a CM1850 cryostat (Leica). 14 μm parasagittal sections were processed for immunohistochemistry.

For double immunofluorescence experiments, PKCα or PKCγ were labeled with rabbit anti-PKCα (1: 100, Cat. no. ab4124, Abcam) or rabbit anti-PKCγ (1: 500, Cat. no. ab71558, Abcam) and goat anti-rabbit Alexa488-conjugated secondary antibody (1: 200, Ref. no. A11059, Life Technologies Invitrogen), while Purkinje neurons were labeled with mouse anti-calbindin (1: 1000, Cat. no. C9848, Sigma-Aldrich) and goat anti-mouse Alexa594-conjugated antibody (1: 200, Ref. no. A11005, Life Technologies Invitrogen). Sections were imaged using a FV500 Olympus Confocal Microscope at 60× magnification and single-plane images were obtained. Image acquisition settings were kept consistent for all samples prepared with a specific set of antibodies to allow for comparison between genotypes. Sample preparation was performed and images were obtained with experimenter blind to genotype.

For molecular layer thickness measurements, sections were prepared by the same method as described above. Purkinje neurons were labeled with mouse anti-calbindin (1: 1000, Cat. no. C9848, Sigma-Aldrich) and goat anti-mouse Alexa488 conjugated secondary antibody (1: 200, Ref. no. A11001, Life Technologies Invitrogen). Sections were imaged using an Axioskop 2 plus microscope (Zeiss) at either 10× or 20× magnification. Measurements were performed using cellSens Standard image analysis software (Olympus). Sample preparation was performed and images were obtained with experimenter blind to genotype.

Molecular layer thickness measurements

Measurement of molecular layer thickness was performed as described previously (23). A line was drawn to measure 100 μm from the depth of the primary fissure along the length of the fissure. From the end of this line, a line was drawn to measure the distance to the nearest Purkinje neuron cell body in lobule V or VI. Measurements of molecular layer thickness were performed in two sections per animal, and reported molecular layer thickness for each animal is the mean of these two measurements. Molecular layer thickness measurement was performed with experimenter blind to genotype.

Paraffin-fixed mouse immunohistochemistry

Mice were anesthetized with isoflurane and brains were removed and fixed in 1% paraformaldehyde in PBS. Subsequently, brains were embedded in paraffin. 4 μm parasagittal sections were prepared.

Slides were hydrated by performing xylene rinses followed by ethanol gradient incubation. Subsequently, 10 mM sodium citrate antigen retrieval was performed by microwave boiling for 5 min. Tissue was then processed for immunohistochemistry. PKC substrate phosphorylation was labeled with rabbit anti-Phospho-(Ser) PKC substrate antibody (1: 200, Cat. no. 2261, Cell Signaling) and goat anti-rabbit Alexa488-conjugated secondary antibody (1: 200, Ref. no. A11059, Life Technologies Invitrogen). Purkinje neurons were labeled with mouse anti-calbindin (1: 1000, Cat. no. C9848, Sigma-Aldrich) and goat anti-mouse Alexa594-conjugated secondary antibody (1: 200, Ref. no. A11005, Life Technologies Invitrogen). The anterior cerebellar vermis in the sections was imaged using a FV500 Olympus Confocal Microscope at 60× magnification and single-plane images were obtained.

Paraffin-fixed human autopsy tissue immunofluorescence

For all immunohistochemistry using human autopsy tissue, 4 μm thick sections were prepared from paraffin-embedded human cerebellar tissue blocks. 11/12 SCA1 specimens were obtained from A. Koeppen, 1/12 SCA1 specimens were obtained from the University of Michigan Brain Bank and 7/7 age-matched healthy control specimens were obtained from the University of Michigan Brain Bank. 7/7 MSA specimens and 7/7 age-matched AD control specimens were obtained from the University of Michigan Brain Bank. Slides were hydrated by performing xylene rinses followed by ethanol gradient incubation. Subsequently, 10 mM sodium citrate antigen retrieval was performed by microwave boiling for 5 min. Tissue was then processed for immunohistochemistry. PKC substrate phosphorylation was labeled with rabbit anti-Phospho-(Ser) PKC

substrate antibody (1: 200, Cat. no. 2261, Cell Signaling) and goat anti-rabbit Alexa488-conjugated secondary antibody (1: 200, Ref. no. A11059, Life Technologies Invitrogen). Purkinje neurons were labeled with mouse anti-calbindin (1: 1000, Cat. no. C9848, Sigma-Aldrich) and goat anti-mouse Alexa594-conjugated secondary antibody (1: 200, Ref. no. A11005, Life Technologies Invitrogen). Sections were imaged using a FV500 Olympus Confocal Microscope at 60× magnification and single-plane images were obtained. Image acquisition settings were kept consistent for all samples to allow for comparison between patients and controls. Sample preparation was performed and images were obtained with experimenter blind to patient disease status.

For each patient and age-matched control, Purkinje neurons were identified as calbindin positive cells whose somata were located in the Purkinje neuron layer. A total of six images of individual Purkinje neurons were obtained for each patient or control, although for some MSA patients there were few surviving Purkinje neurons and it was not possible to obtain six images, in which case no fewer than four images were obtained. To reduce bias, images were obtained in areas were Purkinje neurons showed strong calbindin signal. Images were obtained with experimenter blind to patient disease status.

Analysis of human autopsy tissue immunofluorescence images

In SCA1 and age-matched healthy control tissue, measurements of average staining intensity for both phosphorylated PKC substrate staining and calbindin staining were performed in the soma. Measurements in each cell reflect the average intensity of a circular area encompassing the soma. Measurements were performed with experimenter blind to sample disease status.

For each Purkinje neuron from a given individual, a phosphorylated PKC substrate-to-calbindin intensity ratio was calculated, and in all graphs reporting these ratios each data point represents the mean of these ratios calculated from the four to six images obtained from a single patient. In all graphs where calbindin or phosphorylated PKC substrate intensity is reported, each data point similarly represents the mean of individual measurements from four to six images obtained from each patient. Error bars represent the standard error of the mean for those measurements within a given patient. Lines indicating the mean intensity ratio value or mean intensity across all patients of a group are also included. Statistics reflect a two-way ANOVA analysis, with statistical significance indicating whether there was a statistically significant effect of disease state on phosphorylated PKC substrate-to-calbindin intensity ratio, phosphorylated PKC substrate intensity or calbindin intensity.

RNA isolation and quantitative real-time PCR

Mice were euthanized following anesthesia with isoflurane, and cerebella were removed and flash frozen in liquid nitrogen. Tissue was stored at −80°C until the time of processing. Total RNA from each harvested mouse cerebellum was extracted using Trizol Reagent (Invitrogen) and subsequently purified using the RNeasy mini kit (Qiagen) following the manufacturer's instructions. cDNA was synthesized from 1 μg of purified RNA using the iScript cDNA synthesis kit (cat. no. 1708891, Bio-Rad). Quantitative real-time PCR assays were performed using the iQ SYBR Green Supermix (cat. no. 1708880, Bio-Rad) in a MyiQ Single Color Real-Time PCR Detection System (Bio-Rad), with each reaction performed at a 20 μl sample volume in an iCycler iQ PCR 96-well Plate (Bio-Rad) sealed with Microseal optical sealing tape (Bio-Rad). The relative amount of transcript mRNA was determined using the comparative C_t method for quantitation (74) with *Actb* mRNA serving as the reference gene. C_t values for each sample were obtained in triplicate and averaged for statistical comparisons. The primers used for qRT-PCR are listed as follows: (1) *Dagla* (forward: CAC CTT CGT CAA GCT GAG AG), (reverse: AGA GGA ACA CTT TTA GAC GGC), and (2) *Actb* (forward: CGG TTC CGA TGC CCT GAG GCT CTT), (reverse: CGT CAC ACT TCA TGA TGG AAT TGA).

Electrophysiology

Solutions

Artificial CSF (aCSF) containing the following (in mM): 125 NaCl, 3.5 KCl, 26 $NaHCO_3$, 1.25 NaH_2PO_4, 2 $CaCl_2$, 1 $MgCl_2$ and 10 glucose (osmolarity 295 mOsm) was continuously bubbled with carbogen (95% 0_2/5% CO_2) to achieve a pH of 7.4. For all recordings, pipettes were filled with internal recording solution containing the following (in mM): 119 K Gluconate, 2 Na gluconate, 6 NaCl, 2 $MgCl_2$, 0.9 EGTA, 10 HEPES, 14 tris–phosphocreatine, 4 MgATP, 0.3 tris–GTP, pH 7.3, osmolarity 290 mOsm.

Preparation of brain slices for electrophysiological recordings

Mice were anesthetized by isofluorane inhalation, decapitated and the brains were submerged in pre-warmed (33°C) aCSF. Slices were prepared in aCSF held at 32.5–34°C on a VT1200 vibratome (Leica). Slices were prepared to a thickness of 300 μm and incubated in continuously carbogen (95% 0_2/5% CO_2)-bubbled aCSF for 45 min at 33°C. Slices were subsequently stored in continuously carbon-bubbled aCSF at room temperature until use. For recordings, slices were placed in a recording chamber and continuously perfused with carbogen-bubbled ACSF at 33°C with a flow rate of 2–3 ml/min.

Patch clamp recordings

Purkinje neurons from lobules II–V were identified for patch clamp recordings in parasagittal cerebellar slices using a 40× water-immersion objective and Eclipse FN1 upright microscope (Nikon) with infrared differential interference contrast (IR-DIC) optics that were visualized using NIS Elements image analysis software (Nikon). Borosilicate glass patch pipettes were pulled with resistances of 3–5 MΩ. Recordings were made 1–5 h after slice preparation in a recording chamber that was continuously perfused with carbogen-bubbled ACSF at 33°C at a flow rate of 2–3 ml/min. Data were acquired using an Axon CV-7B headstage amplifier, Axon Multiclamp 700B amplifier, Digidata 1440A interface and pClamp-10 software (MDS Analytical Technologies). In all cases, acquired data were digitized at 100 kHz. Voltage data were acquired in current-clamp mode with bridge balance compensation and filtered at 2 kHz. Cells were rejected if the series resistance changed by >20% during the course of recording. Whole-cell somatic recordings were rejected if the series resistance rose above 15 MΩ, with the majority of recordings showing a series resistance of <10 MΩ. All voltages were corrected for a liquid junction potential of +10 mV (75).

Recordings to determine the current threshold for eliciting dendritic calcium spikes were performed as described above, but in aCSF containing 1 μM tetrodotoxin (Tocris Bioscience).

Analysis of cell capacitance

Whole-cell capacitance was measured using K-gluconate-based internal solution and analysed as described previously (23). Briefly, capacitative transients were obtained in voltage-clamp

mode using 1 s steps to −70 mV from a holding potential of −80 mV. The whole-cell capacitance was calculated as the area underneath the capacitative transient following offline correction for input resistance.

Analysis of baseline firing properties

Analysis of baseline firing properties was performed using Clampfit 10.2 (MDS Analytical Technologies). Firing frequency and coefficient of variation (CV) calculations were performed using a single 10 second trace obtained in the cell-attached recording configuration ∼3 min after formation of a stable seal. CV was calculated as follows:

$$\mathrm{CV} = \frac{\text{Standard deviation of interspike interval}}{\text{Mean interspike interval}}$$

Analysis of the AHP was performed using a single 10 second trace obtained ∼1 min after break-in. To calculate the AHP for each neuron, the minima for each spike in the trace were determined using the antipeak function of Clampfit, and the mean of those minima was reported as the AHP for each neuron.

Input resistance for each cell was calculated by generating an input–output curve for membrane potential versus injected current. This input–output curve encompassed only membrane potential measurements between −80 and −75 mV.

Analysis of dendritic calcium spike threshold

Input resistance for each cell was calculated by generating an input–output curve for membrane potential versus injected current. This input–output curve encompassed only membrane potential measurements between −80 and −75 mV in an effort to minimize the influence of dendritic excitability on measurement of input resistance. This method is consistent with previous studies using the calcium spike method to measure intrinsic dendritic excitability (55).

Chemicals

Reagents and chemical were obtained from Sigma-Aldrich unless or otherwise specified.

Statistical analysis

Statistical tests are described in the figure legends for all data. Data are expressed as mean ± S.E.M. unless or otherwise specified. Sample numbers are included in each panel, with the number of cells (n) or number of animals (N) included where appropriate. Studies were powered and analysis was performed assuming unequal variance between groups. Statistical significance for all Student's t-test analysis was defined as $P < 0.05$. For one-way ANOVA with Holm-Sidak multiple comparison test, adjusted $P < 0.05$ was considered statistically significant, and presented P values are adjusted P values. For two-way ANOVA, statistical significance was defined as $P < 0.05$. Data were analyzed using SigmaPlot (Systat Software), GraphPad Prism (GraphPad) and Excel (Microsoft).

Supplementary Material

Supplementary Material is available at *HMG* online.

Acknowledgements

We thank Dr Arnulf Koeppen for providing autopsy tissue slides from SCA1 patients. We also thank the University of Michigan Brain Bank and Matthew Perkins for providing autopsy tissue slides from an SCA1 patient, age-matched healthy controls, MSA patients and AD patients. We thank William Dauer for helpful comments and suggestions, and James Dell'Orco, Annie Zalon, Alexi Vasbinder, Mandy Rutteman, and Allison Sylvia for technical support.

Conflict of Interest statement. None declared.

Funding

This work was supported by the NIH R01NS085054 (V.G.S.), the NIH T32GM007863 (R.C.), the NIH R37NS033123 (S.M.P.) the NIH R01NS097903 (S.M.P), the National Ataxia Foundation Research Post-Doctoral Fellowship Award (R.C.), The Netherlands Organization for Medical Sciences (C.I.D.Z.), Life Sciences (C.I.D.Z.), and ERC-adv, ERC-POC of the EU (C.I.D.Z.).

References

1. Durr, A. (2010) Autosomal dominant cerebellar ataxias: polyglutamine expansions and beyond. *Lancet Neurol.*, **9**, 885–894.
2. Shakkottai, V.G. and Fogel, B.L. (2013) Clinical neurogenetics: autosomal dominant spinocerebellar ataxia. *Neurol. Clin.*, **31**, 987–1007.
3. Paulson, H.L., Shakkottai, V.G., Clark, H.B. and Orr, H.T. (2017) Polyglutamine spinocerebellar ataxias - from genes to potential treatments. *Nat. Rev. Neurosci.*, **18**, 613–626.
4. Shakkottai, V.G. and Paulson, H.L. (2009) Physiologic alterations in ataxia: channeling changes into novel therapies. *Arch. Neurol.*, **66**, 1196–1201.
5. Huang, F.L., Yoshida, Y., Nakabayashi, H., Young, W.S., 3rd. and Huang, K.P. (1988) Immunocytochemical localization of protein kinase C isozymes in rat brain. *J. Neurosc.*, **8**, 4734–4744.
6. Sun, M.K. and Alkon, D.L. (2014) The "memory kinases": roles of PKC isoforms in signal processing and memory formation. *Prog. Mol. Biol. Trans. Sci.*, **122**, 31–59.
7. Hirai, H. (2018) Protein kinase C in the cerebellum: its significance and remaining conundrums. *Cerebellum*, **17**, 23–27.
8. Metzger, F. and Kapfhammer, J.P. (2000) Protein kinase C activity modulates dendritic differentiation of rat Purkinje cells in cerebellar slice cultures. *Eur. J. Neurosci.*, **12**, 1993–2005.
9. Yabe, I., Sasaki, H., Chen, D.H., Raskind, W.H., Bird, T.D., Yamashita, I., Tsuji, S., Kikuchi, S. and Tashiro, K. (2003) Spinocerebellar ataxia type 14 caused by a mutation in protein kinase C gamma. *Arch. Neurol.*, **60**, 1749–1751.
10. van de Warrenburg, B.P., Verbeek, D.S., Piersma, S.J., Hennekam, F.A., Pearson, P.L., Knoers, N.V., Kremer, H.P. and Sinke, R.J. (2003) Identification of a novel SCA14 mutation in a Dutch autosomal dominant cerebellar ataxia family. *Neurology*, **61**, 1760–1765.
11. Chen, D.H., Brkanac, Z., Verlinde, C.L., Tan, X.J., Bylenok, L., Nochlin, D., Matsushita, M., Lipe, H., Wolff, J. and Fernandez, M. (2003) Missense mutations in the regulatory domain of PKC gamma: a new mechanism for dominant nonepisodic cerebellar ataxia. *Am. J. Hum. Genet.*, **72**, 839–849.
12. Brkanac, Z., Bylenok, L., Fernandez, M., Matsushita, M., Lipe, H., Wolff, J., Nochlin, D., Raskind, W.H. and Bird, T.D. (2002) A

new dominant spinocerebellar ataxia linked to chromosome 19q13.4-qter. *Arch. Neurol.*, **59**, 1291–1295.
13. Ji, J., Hassler, M.L., Shimobayashi, E., Paka, N., Streit, R. and Kapfhammer, J.P. (2014) Increased protein kinase C gamma activity induces Purkinje cell pathology in a mouse model of spinocerebellar ataxia 14. *Neurobiol. Dis.*, **70**, 1–11.
14. Seki, T., Adachi, N., Ono, Y., Mochizuki, H., Hiramoto, K., Amano, T., Matsubayashi, H., Matsumoto, M., Kawakami, H., Saito, N. *et al.* (2005) Mutant protein kinase Cgamma found in spinocerebellar ataxia type 14 is susceptible to aggregation and causes cell death. *J. Biol. Chem.*, **280**, 29096–29106.
15. Shuvaev, A.N., Horiuchi, H., Seki, T., Goenawan, H., Irie, T., Iizuka, A., Sakai, N. and Hirai, H. (2011) Mutant PKCgamma in spinocerebellar ataxia type 14 disrupts synapse elimination and long-term depression in Purkinje cells in vivo. *J. Neurosci.*, **31**, 14324–14334.
16. Adachi, N., Kobayashi, T., Takahashi, H., Kawasaki, T., Shirai, Y., Ueyama, T., Matsuda, T., Seki, T., Sakai, N. and Saito, N. (2008) Enzymological analysis of mutant protein kinase Cgamma causing spinocerebellar ataxia type 14 and dysfunction in Ca2+ homeostasis. *J. Biol. Chem.*, **283**, 19854–19863.
17. Bettencourt, C., Ryten, M., Forabosco, P., Schorge, S., Hersheson, J., Hardy, J. and Houlden, H. and United Kingdom Brain Expression Consortium. (2014) Insights from cerebellar transcriptomic analysis into the pathogenesis of ataxia. *JAMA Neurol.*, **71**, 831–839.
18. Desai, R., Kronengold, J., Mei, J., Forman, S.A. and Kaczmarek, L.K. (2008) Protein kinase C modulates inactivation of Kv3.3 channels. *J. Biol. Chem.*, **283**, 22283–22294.
19. Matter, N., Ritz, M.F., Freyermuth, S., Rogue, P. and Malviya, A.N. (1993) Stimulation of nuclear protein kinase C leads to phosphorylation of nuclear inositol 1,4,5-trisphosphate receptor and accelerated calcium release by inositol 1,4,5-trisphosphate from isolated rat liver nuclei. *J. Biol. Chem.*, **268**, 732–736.
20. Hourez, R., Servais, L., Orduz, D., Gall, D., Millard, I., de Kerchove d'Exaerde, A., Cheron, G., Orr, H.T., Pandolfo, M. and Schiffmann, S.N. (2011) Aminopyridines correct early dysfunction and delay neurodegeneration in a mouse model of spinocerebellar ataxia type 1. *J. Neurosci.*, **31**, 11795–11807.
21. Clark, H.B., Burright, E.N., Yunis, W.S., Larson, S., Wilcox, C., Hartman, B., Matilla, A., Zoghbi, H.Y. and Orr, H.T. (1997) Purkinje cell expression of a mutant allele of SCA1 in transgenic mice leads to disparate effects on motor behaviors, followed by a progressive cerebellar dysfunction and histological alterations. *J. Neurosci.*, **17**, 7385–7395.
22. Price, L.S., Langeslag, M., ten Klooster, J.P., Hordijk, P.L., Jalink, K. and Collard, J.G. (2003) Calcium signaling regulates translocation and activation of Rac. *J. Biol. Chem.*, **278**, 39413–39421.
23. Dell'Orco, J.M., Wasserman, A.H., Chopra, R., Ingram, M.A., Hu, Y.S., Singh, V., Wulff, H., Opal, P., Orr, H.T. and Shakkottai, V.G. (2015) Neuronal atrophy early in degenerative ataxia is a compensatory mechanism to regulate membrane excitability. *J. Neurosci.*, **35**, 11292–11307.
24. Matsuda, S., Mikawa, S. and Hirai, H. (2002) Phosphorylation of serine-880 in GluR2 by protein kinase C prevents its C terminus from binding with glutamate receptor-interacting protein. *J. Neurochem.*, **73**, 1765–1768.
25. Lambolez, B., Audinat, E., Bochet, P., Crepel, F. and Rossier, J. (1992) AMPA receptor subunits expressed by single Purkinje cells. *Neuron*, **9**, 247–258.
26. Servadio, A., Koshy, B., Armstrong, D., Antalffy, B., Orr, H.T. and Zoghbi, H.Y. (1995) Expression analysis of the ataxin-1 protein in tissues from normal and spinocerebellar ataxia type 1 individuals. *Nat. Genet.*, **10**, 94–98.
27. Rosse, C., Linch, M., Kermorgant, S., Cameron, A.J., Boeckeler, K. and Parker, P.J. (2010) PKC and the control of localized signal dynamics. *Nat. Rev. Mol. Cell Biol.*, **11**, 103–112.
28. Barmack, N.H., Qian, Z. and Yoshimura, J. (2000) Regional and cellular distribution of protein kinase C in rat cerebellar Purkinje cells. *J. Comp. Neurol.*, **427**, 235–254.
29. Goto, M.M., Romero, G.G. and Balaban, C.D. (1997) Transient changes in flocculonodular lobe protein kinase C expression during vestibular compensation. *J. Neurosci.*, **17**, 4367–4381.
30. Skinner, P.J., Vierra-Green, C.A., Clark, H.B., Zoghbi, H.Y. and Orr, H.T. (2001) Altered trafficking of membrane proteins in Purkinje cells of SCA1 transgenic mice. *Am. J. Pathol.*, **159**, 905–913.
31. Inoue, T., Lin, X., Kohlmeier, K.A., Orr, H.T., Zoghbi, H.Y. and Ross, W.N. (2001) Calcium dynamics and electrophysiological properties of cerebellar Purkinje cells in SCA1 transgenic mice. *J. Neurophysiol.*, **85**, 1750–1760.
32. Power, E.M., Morales, A. and Empson, R.M. (2016) Prolonged type 1 metabotropic glutamate receptor dependent synaptic signaling contributes to spino-cerebellar ataxia type 1. *J. Neurosc.*, **36**, 4910–4916.
33. Shuvaev, A.N., Hosoi, N., Sato, Y., Yanagihara, D. and Hirai, H. (2017) Progressive impairment of cerebellar mGluR signalling and its therapeutic potential for cerebellar ataxia in spinocerebellar ataxia type 1 model mice. *J. Physiol.*, **595**, 141–164.
34. Antal, C.E. and Newton, A.C. (2014) Tuning the signalling output of protein kinase C. *Biochem. Soc. Trans.*, **42**, 1477–1483.
35. Tsuruno, S. and Hirano, T. (2007) Persistent activation of protein kinase Calpha is not necessary for expression of cerebellar long-term depression. *Mol. Cell. Neurosci.*, **35**, 38–48.
36. De Zeeuw, C.I., Hansel, C., Bian, F., Koekkoek, S.K., van Alphen, A.M., Linden, D.J. and Oberdick, J. (1998) Expression of a protein kinase C inhibitor in Purkinje cells blocks cerebellar LTD and adaptation of the vestibulo-ocular reflex. *Neuron*, **20**, 495–508.
37. Pulst, S.M., Nechiporuk, A., Nechiporuk, T., Gispert, S., Chen, X.N., Lopes-Cendes, I., Pearlman, S., Starkman, S., Orozco-Diaz, G., Lunkes, A. *et al.* (1996) Moderate expansion of a normally biallelic trinucleotide repeat in spinocerebellar ataxia type 2. *Nat. Genet.*, **14**, 269–276.
38. Hansen, S.T., Meera, P., Otis, T.S. and Pulst, S.M. (2013) Changes in Purkinje cell firing and gene expression precede behavioral pathology in a mouse model of SCA2. *Hum. Mol. Genet.*, **22**, 271–283.
39. Liu, J., Tang, T.S., Tu, H., Nelson, O., Herndon, E., Huynh, D.P., Pulst, S.M. and Bezprozvanny, I. (2009) Deranged calcium signaling and neurodegeneration in spinocerebellar ataxia type 2. *J. Neurosci.*, **29**, 9148–9162.
40. Papp, M.I., Kahn, J.E. and Lantos, P.L. (1989) Glial cytoplasmic inclusions in the CNS of patients with multiple system atrophy (striatonigral degeneration, olivopontocerebellar atrophy and Shy-Drager syndrome). *J. Neurol. Sci.*, **94**, 79–100.
41. Andersen, K., Andersen, B.B. and Pakkenberg, B. (2012) Stereological quantification of the cerebellum in patients with Alzheimer's disease. *Neurobiol. Aging*, **33**, 197.e11–20. doi:10.1016/j.neurobiolaging.2010.06.013.
42. Thal, D.R., Rub, U., Orantes, M. and Braak, H. (2002) Phases of A beta-deposition in the human brain and its relevance for the development of AD. *Neurology*, **58**, 1791–1800.
43. Kasumu, A.W., Hougaard, C., Rode, F., Jacobsen, T.A., Sabatier, J.M., Eriksen, B.L., Strøbæk, D., Liang, X., Egorova, P., Vorontsova, D. *et al.* (2012) Selective positive modulator of calcium-activated potassium channels exerts beneficial effects in a mouse model of spinocerebellar ataxia type 2. *Chem. Biol.*, **19**, 1340–1353.

44. Hoebeek, F.E., Stahl, J.S., van Alphen, A.M., Schonewille, M., Luo, C., Rutteman, M., van den Maagdenberg, A.M., Molenaar, P.C., Goossens, H.H., Frens, M.A. *et al.* (2005) Increased noise level of Purkinje cell activities minimizes impact of their modulation during sensorimotor control. *Neuron*, **45**, 953–965.
45. Shakkottai, V.G., do Carmo Costa, M., Dell'Orco, J.M., Sankaranarayanan, A., Wulff, H. and Paulson, H.L. (2011) Early changes in cerebellar physiology accompany motor dysfunction in the polyglutamine disease spinocerebellar ataxia type 3. *J. Neurosci.*, **31**, 13002–13014.
46. Mark, M.D., Krause, M., Boele, H.-J., Kruse, W., Pollok, S., Kuner, T., Dalkara, D., Koekkoek, S., De Zeeuw, C.I. and Herlitze, S. (2015) Spinocerebellar ataxia type 6 protein aggregates cause deficits in motor learning and cerebellar plasticity. **35**, 8882–8895.
47. Egorova, P.A., Zakharova, O.A., Vlasova, O.L. and Bezprozvanny, I.B. (2016) In vivo analysis of cerebellar Purkinje cell activity in SCA2 transgenic mouse model. *J. Neurophysiol.*, **115**, 2840–2851.
48. Mao, J., Wang, X., Chen, F., Wang, R., Rojas, A., Shi, Y., Piao, H. and Jiang, C. (2004) Molecular basis for the inhibition of G protein-coupled inward rectifier K(+) channels by protein kinase C. *Proc. Natl. Acad. Sci. U.S.A.*, **101**, 1087–1092.
49. Williams, A.D., Jung, S. and Poolos, N.P. (2015) Protein kinase C bidirectionally modulates Ih and hyperpolarization-activated cyclic nucleotide-gated (HCN) channel surface expression in hippocampal pyramidal neurons. *J. Physiol.*, **593**, 2779–2792.
50. Trebak, M., Hempel, N., Wedel, B.J., Smyth, J.T., Bird, G.S. and Putney, J.W. Jr. (2004) Negative regulation of TRPC3 channels by protein kinase C-mediated phosphorylation of serine 712. *Mol. Pharmacol.*, **67**, 558–563.
51. Walter, J.T., Alvina, K., Womack, M.D., Chevez, C. and Khodakhah, K. (2006) Decreases in the precision of Purkinje cell pacemaking cause cerebellar dysfunction and ataxia. *Nat. Neurosci.*, **9**, 389–397.
52. Gao, Z., Todorov, B., Barrett, C.F., van Dorp, S., Ferrari, M.D., van den Maagdenberg, A.M., De Zeeuw, C.I. and Hoebeek, F.E. (2012) Cerebellar ataxia by enhanced Ca(V)2.1 currents is alleviated by Ca2+-dependent K+-channel activators in Cacna1a(S218L) mutant mice. *J. Neurosci.*, **32**, 15533–15546.
53. Dell'Orco, J.M., Pulst, S.M. and Shakkottai, V.G. (2017) Potassium channel dysfunction underlies Purkinje neuron spiking abnormalities in spinocerebellar ataxia type 2. *Hum. Mol. Genet.*, **26**, 3935–3945.
54. Llinas, R. and Hess, R. (1976) Tetrodotoxin-resistant dendritic spikes in avian Purkinje cells. *Proc. Natl. Acad. Sci. U.S.A.*, **73**, 2520–2523.
55. Zagha, E., Manita, S., Ross, W.N. and Rudy, B. (2010) Dendritic Kv3.3 potassium channels in cerebellar Purkinje cells regulate generation and spatial dynamics of dendritic Ca2+ spikes. *J. Neurophysiol.*, **103**, 3516–3525.
56. Bushart, D.D., Chopra, R., Singh, V., Murphy, G.G., Wulff, H. and Shakkottai, V.G. (2018) Targeting potassium channels to treat cerebellar ataxia. *Ann. Clin. Trans. Neurol.* doi: 10.1002/acn3.527.
57. Holmes, W.T. and Rall, W. (1992) Electrotonic Models of Neuronal Dendrites and Single Neuron Computation. In McKenna, T.M., Davis, J.L. and Zornetzer, S.F. (eds), *Single Neuron Computation*. Academic Press, Inc., Boston, MA, pp. 7–25.
58. Jorgensen, N.D., Andresen, J.M., Lagalwar, S., Armstrong, B., Stevens, S., Byam, C.E., Duvick, L.A., Lai, S., Jafar-Nejad, P., Zoghbi, H.Y., Clark, H.B. and Orr, H.T. (2009) Phosphorylation of ATXN1 at Ser776 in the cerebellum. *J. Neurochem.*, **110**, 675–686.
59. Shim, H.G., Jang, D.C., Lee, J., Chung, G., Lee, S., Kim, Y.G., Jeon, D.E. and Kim, S.J. (2017) Long-term depression of intrinsic excitability accompanied by synaptic depression in cerebellar Purkinje cells. *J. Neurosci.*, **37**, 5659–5669.
60. Chung, H.J., Steinberg, J.P., Huganir, R.L. and Linden, D.J. (2003) Requirement of AMPA receptor GluR2 phosphorylation for cerebellar long-term depression. *Science (New York)*, **300**, 1751–1755.
61. Jayabal, S., Chang, H.H., Cullen, K.E. and Watt, A.J. (2016) 4-aminopyridine reverses ataxia and cerebellar firing deficiency in a mouse model of spinocerebellar ataxia type 6. *Sci. Rep.*, **6**, 29489.
62. Chopra, R. and Shakkottai, V.G. (2014) Translating cerebellar Purkinje neuron physiology to progress in dominantly inherited ataxia. *Future Neurol.*, **9**, 187–196.
63. De Zeeuw, C.I., Hoebeek, F.E., Bosman, L.W., Schonewille, M., Witter, L. and Koekkoek, S.K. (2011) Spatiotemporal firing patterns in the cerebellum. *Nat. Rev. Neurosci.*, **12**, 327–344.
64. Alvina, K. and Khodakhah, K. (2010) KCa channels as therapeutic targets in episodic ataxia type-2. *J. Neurosci.*, **30**, 7249–7257.
65. Scheuer, T. (2011) Regulation of sodium channel activity by phosphorylation. *Semin. Cell Dev. Biol.*, **22**, 160–165.
66. Park, J.Y., Kang, H.W., Moon, H.J., Huh, S.U., Jeong, S.W., Soldatov, N.M. and Lee, J.H. (2006) Activation of protein kinase C augments T-type Ca2+ channel activity without changing channel surface density. *J. Physiol.*, **577**, 513–523.
67. Nakajo, K. and Kubo, Y. (2005) Protein kinase C shifts the voltage dependence of KCNQ/M channels expressed in *Xenopus oocytes*. *J. Physiol.*, **569**, 59–74.
68. Herlitze, S., Zhong, H., Scheuer, T. and Catterall, W.A. (2001) Allosteric modulation of Ca2+ channels by G proteins, voltage-dependent facilitation, protein kinase C, and Ca(v)beta subunits. *Proc. Natl. Acad. Sci. U.S.A.*, **98**, 4699–4704.
69. Zhu, L., McDavid, S. and Currie, K.P. (2015) "Slow" voltage-dependent inactivation of CaV2.2 calcium channels is modulated by the PKC activator phorbol 12-myristate 13-acetate (PMA). *PLoS One*, **10**, e0134117.
70. Waters, M.F., Minassian, N.A., Stevanin, G., Figueroa, K.P., Bannister, J.P.A., Nolte, D., Mock, A.F., Evidente, V.G.H., Fee, D.B., Müller, U. *et al.* (2006) Mutations in voltage-gated potassium channel KCNC3 cause degenerative and developmental central nervous system phenotypes. *Nat. Genet.*, **38**, 447–451.
71. Zhang, Y. and Kaczmarek, L.K. (2016) Kv3.3 potassium channels and spinocerebellar ataxia. *J. Physiol.*, **594**, 4677–4684.
72. Verbeek, D.S., Knight, M.A., Harmison, G.G., Fischbeck, K.H. and Howell, B.W. (2004) Protein kinase C gamma mutations in spinocerebellar ataxia 14 increase kinase activity and alter membrane targeting. *Brain*, **128**, 436–442.
73. Burright, E.N., Clark, H.B., Servadio, A., Matilla, T., Feddersen, R.M., Yunis, W.S., Duvick, L.A., Zoghbi, H.Y. and Orr, H.T. (1995) SCA1 transgenic mice: a model for neurodegeneration caused by an expanded CAG trinucleotide repeat. *Cell*, **82**, 937–948.
74. Livak, K.J. and Schmittgen, T.D. (2001) Analysis of relative gene expression data using real-time quantitative PCR and the 2(-delta delta C(T)) method. *Methods*, **25**, 402–408.
75. Telgkamp, P. and Raman, I.M. (2002) Depression of inhibitory synaptic transmission between Purkinje cells and neurons of the cerebellar nuclei. *J. Neurosci.*, **22**, 8447–8457.